Medium induced Lorentz symmetry breaking effects in nonlocal Polyakov–Nambu–Jona-Lasinio models

S. Benić,[1] D. Blaschke,[2,3,4] G. A. Contrera,[5,6,7] and D. Horvatić[1]

[1]*Physics Department, Faculty of Science, University of Zagreb, Zagreb 10000, Croatia*
[2]*Institut Fizyki Teoretycznej, Uniwersytet Wrocławski, 50-204 Wrocław, Poland*
[3]*Bogoliubov Laboratory for Theoretical Physics, JINR Dubna, 141980 Dubna, Russia*
[4]*Fakultät für Physik, Universität Bielefeld, 33615 Bielefeld, Germany*
[5]*CONICET, Rivadavia 1917, 1033 Buenos Aires, Argentina*
[6]*IFLP, CONICET—Departamento de Física, UNLP, La Plata, Argentina*
[7]*Gravitation, Astrophysics and Cosmology Group, FCAyG, UNLP, La Plata, Argentina*

(Received 17 June 2013; revised manuscript received 28 October 2013; published 7 January 2014)

In this paper, we detail the thermodynamics of two-flavor nonlocal Polyakov–Nambu–Jona-Lasinio models for different parametrizations of the quark interaction regulators. The structure of the model is upgraded in order to allow for terms in the quark self-energy that violate Lorentz invariance due to the presence of the medium. We examine the critical properties, the phase diagram, and the equation of state. Furthermore, some aspects of the Mott effect for pions and sigma mesons are discussed explicitly within a nonlocal Polyakov–Nambu–Jona-Lasinio model. In particular, we continued the meson polarization function in the complex energy plane. Under certain approximations we were able to extract the imaginary part as a function of the meson energy. We were not able to calculate the dynamical meson mass and therefore resorted to a technical study of the temperature dependence of the meson width by replacing the meson energy with the temperature-dependent spatial meson mass. Our results show that, while the temperature behavior of the meson widths is qualitatively the same for a wide class of covariant regulators, the special case in which the nonlocal interactions are introduced via the instanton liquid model singles out with a drastically different behavior.

DOI: 10.1103/PhysRevD.89.016007 PACS numbers: 11.10.St, 11.10.Wx, 11.30.Rd, 12.39.Ki

I. INTRODUCTION

Temperatures and densities in heavy ion collisions are well above the point at which hadrons maintain their identity. Experimental data from the Relativistic Heavy Ion Collider (RHIC) and LHC provide strong evidence that, beyond a certain temperature, low-energy QCD forms a strongly coupled quark-gluon plasma (QGP) phase [1,2], behaving almost like a perfect fluid of deconfined quark and gluon degrees of freedom. Future facilities like Nuclotron-based Ion Collider Facility at JINR and Facility for Antiproton and Ion Research at GSI will complement these results by studying the region of extreme densities, thereby allowing a detailed account on the whole QCD phase diagram [3,4]. Recent reviews on the phase diagram are given, e.g., in Refs. [5,6].

A strongly interacting theory can be fully addressed in lattice simulations. At present, thermodynamic properties of lattice QCD can be calculated for physical quark masses (for latest results of the Wuppertal–Budapest group, see Ref. [7]). This leads to the important result, already observed several years ago [8,9], that the lattice data below and including the pseudocritical temperature are described by the hadron resonance gas model [10]. These findings are now well established [11].

Because of the sign problem, lattice calculations are still restricted to a narrow range of finite baryon number chemical potential dictated by the convergence radius of Taylor expansion techniques at $\mu = 0$. On the other hand, in continuum studies, concentrated on the low-energy chiral quark sector, a tremendous amount of work has been accomplished in exploring the whole QCD phase diagram. These studies can be roughly separated into classes ranging from the Nambu–Jona Lasinio (NJL) model with local quark interactions [12,13] (see the reviews [14–17] for application to quark matter) to the more fundamental approach to QCD making use of the tower of integral equations for the n-point functions of Euclidean QCD, the Dyson–Schwinger equation (DSE) approach [18–20]. Quark DSEs usually operate on the level of modelling an effective gluon propagator for describing the nonperturbative interaction between quarks and neglecting the ghosts (global color model; see Ref. [21]), although a more complete approach is also being developed; see, e.g., Ref. [22].

A *separable* form of the quark-quark interaction [23–27] bridges the gap between the two approaches, NJL and DSE, giving rise to a nonlocal NJL (nl-NJL) model [28–31]. With this development, the quark propagator entails a dynamical mass and wave function renormalization as is well known from lattice QCD studies; see Ref. [32]. As an additional effect, poles of the quark propagator can be absent from the real axes [24,25,33]. It is well known that the appearance

of, e.g., complex conjugate mass poles (CCMPs) in the propagator provides sufficient criteria for confinement [18,19,24,25,33–36]. Furthermore, nonlocal models do not require additional cutoffs [37] and find no problem in treating anomalies [38]. An alternative way to introduce the nonlocality is inspired by the instanton liquid model (ILM) [24,25,39–42].

Recently, the nl-NJL model was generalized by coupling its chiral quark sector to the Polyakov loop (PL) variable with an appropriate model for the PL potential [43–51]. The most advanced of these nonlocal Polyakov–Nambu–Jona-Lasinio (nl-PNJL) approaches address both scalar and vector quark self-energies, like the QCD DSEs do. It has been demonstrated that these approaches can be embedded in a scheme that aims toward a first principle derivation of a low-energy QCD description capable of addressing both confinement and chiral symmetry breaking crossover transitions [52].

The field-theoretic formulation of such nl-PNJL models provides a natural starting point for developing them further beyond the mean field level to address in particular mesonic correlations[1] [43,45,47,50]. The effective mesonic action obtained by integrating out the quark degrees of freedom reveals its coupling constants as nonlocal vertices. For example, to Gaussian order of the expansion of the fermion determinant, the meson fields can be integrated out, and the result defines complex meson propagators in the rainbow-ladder approximation. Masses and widths that encode information on the medium modification of mesons by the underlying quark-antiquark substructure can be extracted. Therefore, the nl-PNJL and quark (and gluon) models in general are in an interesting position to properly account for the degrees of freedom in both the hadron and the QGP phases, with the underlying physical mechanism for the vanishing of hadronic states from the spectrum in the QGP phase being their dissolution in the continuum of scattering states (the Mott effect) [55–62].

In the present work, we are going to develop the nl-PNJL approach further in three directions. First, we extend the model with wave function renormalization (WFR) in a simple way such that it accommodates the medium-induced Lorentz symmetry breaking (LSB) in the quark propagator invariants. To observe the magnitude of LSB, selected thermodynamic quantities are displayed together with the scenario that employs only Lorentz symmetric current-current interactions [48,51]. More precisely, we compute the quark mean fields at finite temperature and observe that Lorentz symmetry is heavily broken around and above T_c. In addition, we fill a gap in the literature by providing some analytic estimates on the effect of WFR and LSB on the critical properties of nonlocal as well as local NJL models.

Second, we investigate the role of the PL coupling in this context. A strong effect of WFR and LSB is to be seen above the chiral pseudocritical temperature T_c. This leads us to consider the equation of state (EoS) for quark matter, as correlations above could help maintain the EoS well below the Stefan–Boltzmann value even for temperatures up to 0.6–0.8 GeV as observed in lattice QCD [7]. We use three sets of parametrizations for nonlocality provided in Ref. [48]. We demonstrate here for the first time that the behavior of the EoS is much more similar to the one measured in lattice QCD simulations in all these cases only when coupled to the PL.

In our study of LSB, we find that, even though the Lorentz covariance of the propagator is drastically broken above T_c, the bulk thermodynamic properties remain practically untouched. The critical line in the phase diagram and, especially, the critical end point (CEP), as well as the EoS, are affected very little by LSB.

Finally, we develop our model beyond the mean field by taking into account Gaussian fluctuations of the pion and sigma mesons. One novel result is a closed formula for the imaginary part of the meson polarization loop extracted at zero meson momenta, leading to the meson width. By calculating also the meson masses, we are able to make an exploratory study of the Mott effect in a nl-PNJL. Our results are of technical nature exposing a surprising sensitivity to the specific form of the nonlocal interactions. Whereas both the standard nonlocal interaction, inspired by the separable DSE model, and the one inspired by the ILM, are equivalent on the mean-field level, the treatment of fluctuations is somewhat different; see, e.g., Ref. [40]. We find that this difference leads to dramatically different results for the meson widths: in the former case the widths start rising but drop to zero in the high-temperature regime, whereas, in the latter case, they are monotonous functions of the temperature.

We organize this paper as follows. In Sec. II, the nl-NJL model is shorty reviewed, in order to introduce LSB terms. Critical properties are discussed in Sec. III, notably the CEP and the phase diagram, followed by results for the EoS in Sec. IV. Thermodynamics beyond the mean field is developed in Sec. V, whereby details of the mathematical formalism in obtaining the in-medium mesonic polarization function are separated in the Appendix. In Sec. VI, we present our conclusions from the results of these investigations.

II. SETTING UP THE MODEL

Starting point of our investigation is the Euclidean action functional of the nl-NJL model [48]

[1]The description of diquark [53] and baryonic [54] correlations in matter have so far been developed to the level of the nl-NJL approach without coupling them to the PL.

$$S_E = \int d^4x \Big\{ \bar{q}(-i\partial\!\!\!/ + m)q - \frac{G_S}{2}[j_a^S(x) j_a^S(x) + j_p(x) j_p(x)] \Big\}, \tag{1}$$

with currents

$$j_a^S(x) = \int d^4z g(z) \bar{q}\left(x + \frac{z}{2}\right) \Gamma_a q\left(x - \frac{z}{2}\right),$$
$$j_p(x) = \int d^4z f(z) \bar{q}\left(x + \frac{z}{2}\right) \frac{i\overleftrightarrow{\partial\!\!\!/}}{2\kappa_p} q\left(x - \frac{z}{2}\right), \tag{2}$$

where $\Gamma_a = (1, i\gamma_5\boldsymbol{\tau})$, and $\boldsymbol{\tau}$ are Pauli matrices. When calculating the EoS and the meson properties (see Secs. IV and V, respectively), we will be interested also in a version of the nl-PNJL inspired by the ILM model. In this case, only the $j_a^S(x)$ current is present in the action (1) in the form

$$j_a^S(x) = \int d^4y d^4z r(y-x) r(x-z) \bar{q}(y) \Gamma_a q(z). \tag{3}$$

We work with $N_f = 2$, $q = (u, d)^{\mathrm{T}}$. The symbol $\overleftrightarrow{\partial}_\mu$ provides a shorthand for

$$\psi(x) \overleftrightarrow{\partial}_\mu \varphi(y) = \psi(x) \frac{\partial \varphi(y)}{\partial y_\mu} - \frac{\partial \psi(x)}{\partial x_\mu} \varphi(y).$$

The definite shapes of the regulators $g(z)$, $f(z)$, or $r(z)$ in the ILM case will be provided below in momentum space. Physically, they can be thought of as mimicking effective nonlocal 4-quark interactions, or alternatively as wave functions of quark-antiquark correlations (see, e.g., Ref. [63]).

Finite temperature and chemical potential are introduced via the Matsubara formalism [64] analogous to the case of the local NJL model [14–17]. The thermodynamic potential in a mean-field approximation is

$$\Omega = \Omega_{\mathrm{cond}} + \Omega_{\mathrm{kin}}, \tag{4}$$

$$\Omega_{\mathrm{cond}} = \frac{1}{2G_S}(\sigma_1^2 + \kappa_p^2 \sigma_2^2), \tag{5}$$

$$\Omega_{\mathrm{kin}} = -\frac{d_q}{4} T \sum_{n=-\infty}^{\infty} \int \frac{d^3p}{(2\pi)^3} \mathrm{tr}_D \log\,[S^{-1}(\tilde{p}_n)], \tag{6}$$

where tr_D is the Dirac trace, and $d_q = 2 \times 2 \times N_c \times N_f$. The regularization of this divergent quantity is performed as in Ref. [48], providing Ω_{reg}. The full quark propagator is

$$S^{-1}(\tilde{p}_n) = -(\gamma \cdot \tilde{p}_n) A(\tilde{p}_n^2) + B(\tilde{p}_n^2), \tag{7}$$

where $\tilde{p}_n^2 = \mathbf{p}^2 + \tilde{\omega}_n^2$, $\tilde{\omega}_n = \omega_n - i\mu$, $\omega_n = (2n+1)\pi T$, with dressing functions

$$A(p^2) = 1 + \sigma_2 f(p^2), \tag{8}$$

$$B(p^2) = m + \sigma_1 g(p^2), \tag{9}$$

encoding the effect of the background fields (σ_1, σ_2).

For the ILM, the thermodynamic potential on the mean-field level takes the same form, provided that only the scalar channel is kept, i.e., $A(p^2) = 1$, and a replacement $g(p^2) \to r^2(p^2)$ is performed.

This kind of quark propagator is very typical for DSE studies as, e.g., in Ref. [18]. The closest analogy is provided using the separable kernel for the gluon propagator, as in Refs. [25–27]. Then, one can start from the rainbow-ladder approximation [18] of the Cornwall–Jackiw–Tomboulis two-particle-irreducible effective action [65] of the quark sector and introduce a separable gluon propagator in order to obtain an expression [49] constructively very similar to Eq. (4).

The regulators specified in Refs. [46,48] are dubbed set A (Gaussian, without WFR), set B (Gaussian, with WFR), and set C (Lorentzian, with WFR) as described below. As a shorthand, we also adopt the terminology of separable models as used in Refs. [27,49], referring to models without WFR as rank 1 and to those with WFR as rank 2. The three regulator sets are defined as

$$\left.\begin{aligned} g(p^2) &= \exp(-p^2/\Lambda_0^2) \\ f(p^2) &= 0 \end{aligned}\right\} \quad \text{(set A)}, \tag{10}$$

$$\left.\begin{aligned} g(p^2) &= \exp(-p^2/\Lambda_0^2) \\ f(p^2) &= \exp(-p^2/\Lambda_1^2) \end{aligned}\right\} \quad \text{(set B)}, \tag{11}$$

$$\left.\begin{aligned} g(p^2) &= \frac{1+\alpha_z}{1+\alpha_z f_z(p^2)} \frac{\alpha_m f_m(p^2) - m\alpha_z f_z(p^2)}{\alpha_m - m\alpha_z} \\ f(p^2) &= \frac{1+\alpha_z}{1+\alpha_z f_z(p^2)} f_z(p^2) \end{aligned}\right\} \quad \text{(set C)}, \tag{12}$$

where

$$f_m(p^2) = \left[1 + (p^2/\Lambda_0^2)^{3/2}\right]^{-1}, \tag{13}$$

$$f_z(p^2) = [1 + p^2/\Lambda_1^2]^{-5/2}, \tag{14}$$

TABLE I. Parameter sets A–C and the ILM model as used in this work. For further details on sets A–C, see Refs. [46,48], and for the ILM model, see Ref. [40].

	Set A	Set B	Set C	ILM
m [MeV]	5.78	5.7	2.37	5.8
Λ_0 [GeV]	0.752	0.814	0.850	0.902
$G_S\Lambda_0^2$	20.65	32.03	20.818	15.82
Λ_1 [GeV]	⋯	1.034	1.400.0	⋯
κ_p [GeV]	⋯	4.180	6.034	⋯

and $\alpha_m = 309$ MeV, $\alpha_z = -0.3$. For the ILM model, we have

$$\left.\begin{array}{c} r(p^2) = \exp\left(-p^2/2\Lambda_0^2\right) \\ f(p^2) = 0 \end{array}\right\} \quad \text{(ILM)}. \tag{15}$$

All the parameter sets are summarized in Table I.

A. Lorentz symmetry breaking by the medium

As the medium presents a distinct reference frame, Lorentz symmetry is broken. Effects of this breaking are revealed in the richer tensor structures for the Green's functions of the theory, notably the propagators. Here, we explore the possibility of splitting the WFR term in the quark propagator. This is a very well-known effect in DSE studies at finite temperatures and chemical potentials [66,67], see also Ref. [18], through which, for example, the possible existence of plasmino modes above T_c can be explored [68,69].

The residual $O(3)$ symmetry of the medium allows the following structure of the quark propagator[2]:

$$S^{-1}(\tilde{p}_n) = -(\boldsymbol{\gamma}\cdot\mathbf{p})A(\tilde{p}_n^2) - \gamma_4\tilde{\omega}_n C(\tilde{p}_n^2) + B(\tilde{p}_n^2). \tag{16}$$

It is clear that a covariant nl-NJL model interaction $j_p(x)j_p(x)$, see Eq. (1), can only yield $C(p^2) = A(p^2)$ (9). To take into account also the more general possibility $A(p^2) \neq C(p^2)$, we break the $O(4)$ symmetry to $O(3)$ in the interaction itself by modifying the $j_p(x)$ channel

$$j_p j_p \to j_{\mathbf{p}} j_{\mathbf{p}} + j_{p4} j_{p4}, \tag{17}$$

where

$$j_{\mathbf{p}}(x) = \int d^4z f(z)\bar{q}\left(x+\frac{z}{2}\right)\frac{i\overleftrightarrow{\nabla}\boldsymbol{\gamma}}{2\kappa_{\mathbf{p}}}q\left(x-\frac{z}{2}\right), \tag{18}$$

$$j_{p_4}(x) = \int d^4z f(z)\bar{q}\left(x+\frac{z}{2}\right)\frac{i\overleftrightarrow{\partial}_4\gamma_4}{2\kappa_{p4}}q\left(x-\frac{z}{2}\right), \tag{19}$$

with the couplings $\kappa_{\mathbf{p}}$ and κ_{p4} regulating the strength of each term. This modification now preserves only $O(3)$ symmetry and alters the thermodynamic potential (6). The condensate term Ω_{cond} becomes

$$\Omega_{\text{cond}} \to \frac{1}{2G_S}(\sigma_B^2 + \kappa_{\mathbf{p}}^2\sigma_A^2 + \kappa_{p4}^2\sigma_C^2), \tag{20}$$

while the quark propagator in Ω_{kin} goes to Eq. (16). In discussing the effects of LSB, we use for the mean fields the same nomenclature as in Ref. [18], i.e., $\sigma_i (i = A, B, C)$, in order to differentiate from $\sigma_{1,2}$ of the Lorentz symmetric (LS) case. $C(p^2)$ is yet another quark dressing function symbolizing the breakdown of $O(4)$ symmetry $C(p^2) = 1 + \sigma_C f(p^2)$.

Full correspondence with the separable DSE studies in, e.g., Refs. [27,49], is obtained by using $\kappa_{\mathbf{p}}^2/\kappa_{p4}^2 = 3$. To restore the $O(4)$ symmetric form (6) in the vacuum, we must have $\kappa_{\mathbf{p}}^2 = 3\kappa_p^2/4$, $\kappa_{p_4}^2 = \kappa_p^2/4$.

B. Polyakov loop

The PL [71] Φ (and its conjugate $\bar{\Phi}$) represents a nonperturbative pure-glue vacuum response to an infinitely heavy "probe" quark (antiquark). As such, it stands for an order parameter for confinement in accordance with the spontaneous breaking of center symmetry of the gauge group $SU(3)_c$. However, the center symmetry is strictly broken with dynamical quarks winding around the thermal circle as they are bound to respect the antiperiodic boundary conditions.

The PL is introduced as the color trace over a position-independent timelike gluon background field φ_3 in the Polyakov gauge [71], $\Phi = [1 + 2\cos(\varphi_3/T)]/N_c$, which modifies the Matsubara frequencies $\tilde{\omega}_n = \omega_n - i\mu + \lambda_3\varphi_3$, depending on the color state. In the thermodynamic potential, the color trace, as well as the Dirac trace, becomes nontrivial,

$$\Omega_{\text{kin}} = -\frac{d_q}{12}T\sum_{n=-\infty}^{\infty}\int\frac{d^3p}{(2\pi)^3}\text{tr}_{D,C}\,\log\,S^{-1}(\tilde{p}_n). \tag{21}$$

The unregularized mean field thermodynamic potential is then augmented by a gluon mean field potential $\mathcal{U}(\Phi, T)$ to become

$$\Omega = \Omega_{\text{cond}} + \Omega_{\text{kin}} + \mathcal{U}(\Phi, T), \tag{22}$$

[2]Here, we have two vectors at our disposal: the momentum of the particle and the momentum of the medium. Therefore, there may be, in principle, medium-induced tensor forces (see, e.g., Ref. [70]), giving rise to a $\sigma^{\mu\nu}$ term in the propagator. To get this term, one should include a tensor channel in the NJL model, a possibility that we do not consider in this work.

where we choose the logarithmic form of the PL potential $\mathcal{U}(\Phi, T)$ introduced in Ref. [72],

$$\mathcal{U}(\Phi,T)=\left[-\frac{1}{2}a(T)\Phi^2+b(T)\ln(1-6\Phi^2+8\Phi^3-3\Phi^4)\right]T^4, \tag{23}$$

with $a(T)=a_0+a_1(T_0/T)+a_2(T_0/T)^2$, $b(T)=b_3(T_0/T)^3$. The corresponding parameters are $a_0=3.51$, $a_1=-2.47$, $a_2=15.22$, and $b_3=-1.75$. In the present work, we set $T_0=0.27$ GeV.

C. Physical meaning of the mean fields

The σ_B mean field is closely related to the quark condensate $\langle\bar{q}q\rangle$ signalling chiral symmetry breaking. Although in the nl-NJL the mass is a dynamical quantity, depending on quark momentum, σ_B is usually referred to as the mass gap.

The "derivative" mean fields, σ_A and σ_C, provide the quark propagator with a nonzero WFR as seen on the lattice as well as in DSE models. It is very useful to consider the NJL-like limit of the model with $f(p^2)\to\theta(\Lambda_0^2-\mathbf{p}^2)$ and $g(p^2)\to\theta(\Lambda_0^2-\mathbf{p}^2)$. The NJL thermodynamic potential with WFR and LSB can be simply obtained from the one without the WFR given in, e.g., Ref. [17]. While $\Omega_{\rm cond}$ can be directly taken from Eq. (20), the kinetic part is the quasiparticle Fermi gas,

$$\Omega_{\rm kin}=-\frac{d_q}{2}\int\frac{d^3p}{(2\pi)^3}\Big\{E+T\,\log[1+e^{-\beta(E-\mu)}]+T\,\log[1+e^{-\beta(E+\mu)}]\Big\}, \tag{24}$$

where E is given by

$$v_{\rm qp}^2\mathbf{p}^2-E^2+m_{\rm qp}^2=0, \tag{25}$$

and

$$v_{\rm qp}=\frac{A_0}{C_0}=\frac{1+\sigma_A}{1+\sigma_C},\qquad m_{\rm qp}=\frac{B_0}{C_0}=\frac{m+\sigma_B}{1+\sigma_C}, \tag{26}$$

where $A_0=A(0)$, $B_0=B(0)$, and $C_0=C(0)$. The values $1/A_0$ and $1/C_0$ represent WFR. Furthermore, causality requires $v_{\rm qp}\le 1$ (the speed of light) leading to $\sigma_A\le\sigma_C$. This is the first physical manifestation of LSB encoded in the full numerical solutions in the following sections.

The most important use of the PL in NJL models is to suppress quark excitations at low temperatures. In covariant nl-NJL models, remnants of the quark excitations are still present in the complex plane in the confining phase, leading to unphysical thermodynamic behavior. The PL then acts to strongly suppress such states from being thermally excited [73]; see also Sec. IV A.

III. CRITICAL PROPERTIES

In this section, we discuss the effect of the wave function renormalization on the critical coupling for chiral symmetry breaking and the chiral restoration temperature. We restrict ourselves to discuss only sets A–C; the ILM model will become important in the following sections. The following analytical estimates are restricted to the chiral limit and to the case without the PL. Next, solutions of the gap equations with and without LSB effects will be compared. Results show that LSB is more profound around the chiral restoration, in accordance with Ref. [27]. Finally, the influence of LSB on the phase diagram and on the CEP is calculated.

A. Critical coupling analysis

In this subsection, we work in the chiral limit $m=0$. The onset of the chiral transition is controlled by the strength of the scalar channel G_S. For the local NJL with a standard three-dimensional (3D) cutoff Λ_0, the critical value for the coupling is [74]

$$G_S^c\Lambda_0^2=\frac{8\pi^2}{d_q}. \tag{27}$$

One can easily show that the effect of a constant WFR amounts to

$$G_S^c\Lambda_0^2=\frac{8\pi^2}{d_q}A_0^2, \tag{28}$$

where the term $A_0=1+\sigma_2>1$ leads to an increase in the critical coupling.

In rank-1 Gaussian models, we quote [30] the result $G_S^c\Lambda_0^2=4\times 8\pi^2/d_q$, while for rank-2 Gaussian models, (set B) one can obtain a similar expression,

$$G_S^c\Lambda_0^2=4\frac{8\pi^2}{d_q}\frac{1}{\rho\left(\sigma_2,\frac{\Lambda_0^2}{\Lambda_1^2}\right)}, \tag{29}$$

where

$$\rho(a,x)=2\int_0^\infty dy\frac{ye^{-y^2}}{(1+ae^{-xy^2/2})^2}=1-\frac{2a}{1+\frac{x}{2}}+\frac{3a^2}{1+x}+\cdots, \tag{30}$$

and Λ_0 and Λ_1 are the scales of the appropriate regulators; see Eqs. (10)–(15). The second equality provides an expansion in σ_2, valid for $\sigma_2<1$. Then, $\rho<1$, and we have $(G_S^c\Lambda_0^2)_{\text{rank-2}}>(G_S^c\Lambda_0^2)_{\text{rank-1}}$, concluding that the critical coupling is in principle always larger for rank 2 than for rank 1. This is in accord with the above simplified NJL

scenario. If we are to use some reasonable values, say $\Lambda_0 \simeq \Lambda_1$ and $\sigma_2 \sim 0.5$, we have $\rho \simeq 0.6$.

B. Critical line in the phase diagram

Let us now proceed to approximate the influence of wave function renormalization on T_c. In the local model [74], as well as the rank-1 nl-NJL model [30], this is simply given as

$$T_c = \left[\frac{24}{d_q}\left(\frac{1}{G_S^c} - \frac{1}{G_S}\right)\right]^{1/2}, \tag{31}$$

with G_S^c given by their respective values.

With WFR, the analysis is very similar. The quark loop that needs to be evaluated is

$$\left.\frac{\partial^2 \Omega_{\text{kin}}}{\partial \sigma_B^2}\right|_{\sigma_B=0} = -d_q T \sum_{n=-\infty}^{\infty} \int \frac{d^3p}{(2\pi)^3} \frac{g^2(p_n^2)}{\mathbf{p}^2 A^2(p_n^2) + \omega_n^2 C^2(p_n^2)}. \tag{32}$$

We first study a slightly simplified scenario with $A(p^2) = C(p^2)$. Then, the denominator as a function of $z = i\omega_n$ has simple poles at $\pm\mathbf{p}$. For rank 1, these are the only poles. For rank 2 set B, there is also an infinite tower of double poles when $A^2(-z^2 + \mathbf{p}^2) = 0$. We ignore them at this point, by assuming they have a significant effect only after T_c; see Sec. IV. By explicitly evaluating the Matsubara sum, as well as the momenta integral, we obtain

$$T_c \simeq A_0 \left[\frac{24}{d_q}\left(\frac{1}{G_S^c} - \frac{1}{G_S}\right)\right]^{1/2}, \tag{33}$$

with G_S^c given by Eq. (29).

If we suppose that G_S in rank 2 is scaled to G_S in rank 1, just like it is true for G_S^c [see Eq. (29)], and that also, for simplicity, cutoff scales Λ_0 are the same, we conclude that

$$(T_c)_{\text{rank-2}} \simeq A_0 \rho^{1/2}\left(\sigma_2, \frac{\Lambda_0^2}{\Lambda_1^2}\right)(T_c)_{\text{rank-1}},$$

where $\rho(a, x)$ is given in Eq. (30). As $\rho < 1$ and $A_0 > 1$, there occurs a compensation, producing roughly the same temperature as in rank 1. Taking actual values for set B [46,48], we obtain $(T_c)_{\text{rank-2}} \simeq 1.08(T_c)_{\text{rank-1}}$.

The first nontrivial effect of LSB on T_c can be established by studying Eq. (32) for poles $\pm v_{\text{qp}}\mathbf{p}$. It is an easy task to show that

$$(T_c)^{\text{LSB}}_{\text{rank-2}} \simeq v_{\text{qp}}^{1/2} (T_c)^{\text{LS}}_{\text{rank-2}}, \tag{34}$$

where $(T_c)^{\text{LS}}_{\text{rank-2}}$ is provided by the previous equation. Therefore, LSB leads to a decrease of the critical temperature.

Introducing the chemical potential can lead to a change in the critical behavior— from second order at low μ to a first-order transition at high μ. We ask for a simplest possible analytic estimate on the effect of WFR and LSB on the phase transition line and on the CEP. Therefore, we will show explicit analytic results only in the local NJL limit. A high-temperature expansion [75] of Eq. (24) leads to a Landau form of the thermodynamic potential, i.e.,

$$\Omega \simeq -\frac{1}{2} D(T,\mu)\sigma_B^2 + \frac{1}{4} F(T,\mu)\sigma_B^4. \tag{35}$$

The Landau coefficients, $D(T,\mu)$ and $F(T,\mu)$, are

$$D(T,\mu) = -\frac{1}{G_S} + \frac{1}{v_{\text{qp}}^3}\frac{1}{C_0^2}\frac{1}{G_S^c} + \frac{d_q}{8\pi^2}\frac{T^2}{v_{\text{qp}}^3}\left(\frac{\pi^2}{3} + \frac{\mu^2}{T^2}\right)\frac{1}{C_0^2}, \tag{36}$$

$$F(T,\mu) \simeq \frac{d_q}{8\pi^2}\frac{1}{v_{\text{qp}}^3}\left[\log\frac{\Lambda_0}{2\pi T} + \gamma - 1 + \frac{7}{2}\zeta(3)\left(\frac{\mu}{2\pi T}\right)^2\right]\frac{1}{C_0^4}, \tag{37}$$

with G_S^c given by Eq. (27). We should warn that, while Eq. (36) is exact, in Eq. (37) we restrict ourselves only to the first nontrivial term in the μ/T expansion [75].

Requiring $D(T,\mu) = 0$ gives us the behavior of the critical line $T_c(\mu)$ at $\mu/T \ll 1$. A canonical form is established by

$$\frac{T_c(\mu)}{T_c(0)} = 1 - \kappa\left(\frac{\mu}{T_c(\mu)}\right)^2, \tag{38}$$

where κ denotes the curvature of the critical line. The importance of this quantity lies in the fact that it can be measured on the lattice; see, e.g., Ref. [76]. We can immediately see that introducing WFR, as well as LSB, does not change the curvature, the latter being simply $\kappa = 3/\pi^2$. The same can be conjectured also for the nonlocal rank-1 models because the medium component of Eq. (36) is governed by the singularities of the quark propagator. At $\sigma_1 = 0$, the nonlocal rank-1 model has the same singularities as the local one. However, as was already mentioned, rank-2 models have additional singularities in the WFR term; see Eq. (32), which might then alter the medium part in Eq. (36). In fact, a full numerical study [77] shows that the general effect of WFR is to increase κ. From the physical point of view, this is to be expected, since the singularities effectively act as additional "degrees of freedom."

The CEP can be inferred by simultaneously requiring $D(T,\mu) = 0$ and $F(T,\mu) = 0$. Restricting to keep only the $\sim(\mu/T)^2$ term in Eq. (37) limits the discussion somewhat by excluding a possible low-T, high-μ CEP. On the other hand, by inserting Eq. (36) into Eq. (37), we are lead to a simple condition on T_{CEP},

$$-\log\frac{T_{\rm CEP}}{\Lambda_0}+\frac{7\zeta(3)}{24}\frac{T_c^2(0)}{T_{\rm CEP}^2}=\frac{7\zeta(3)}{24}+\log(2\pi)+1-\gamma\equiv R, \tag{39}$$

which can be easily analyzed. Now, we may estimate the influence of WFR and LSB on the CEP. First of all, the right-hand side of the last equation is a pure number, $R\simeq 2.61$. Second, since we know that $T_c(0)\simeq v_{\rm qp}^{1/2}T_c^{\rm LS}(0)$, the quadratically divergent term will be somewhat stronger, further decreasing $T_{\rm CEP}$. If we take this term to be the dominant one, we obtain

$$T_{\rm CEP}^{\rm LSB}\simeq v_{\rm qp}^{1/2}T_{\rm CEP}^{\rm LS}=\sqrt{\frac{7\zeta(3)}{24R}}v_{\rm qp}^{1/2}T_c^{\rm LS}(0)\simeq 0.37\,v_{\rm qp}^{1/2}T_c^{\rm LS}(0). \tag{40}$$

Within this approximation, there is no influence of the LS version of the WFR channel on the CEP. On the other hand, we may conclude that the first estimate on the influence of the LSB on the CEP is that the CEP goes to lower T and, consequently, to higher μ. Owing to the fact that the presented analysis is rather crude, and formally confined to $\mu/T\ll 1$, we conclude that deviations might be even larger and get further increased in the rank-2 nonlocal case. A full numerical study in nonlocal models, see, e.g., Refs. [48,77], supports this conjecture.

C. Splitting of σ_A and σ_C and the phase diagram

In Sec. II A, we argued for the possibility of the most general structure of the quark propagator (16). The numerical results obtained from the minimization of the thermodynamic potential are shown in Fig. 1. By comparing the mass gaps, it is plain that there is barely an influence.

On the contrary, in Fig. 1, there is a clear difference between the σ_A and σ_C mean fields defining a region in which $O(4)$ symmetry is violated. This difference is a

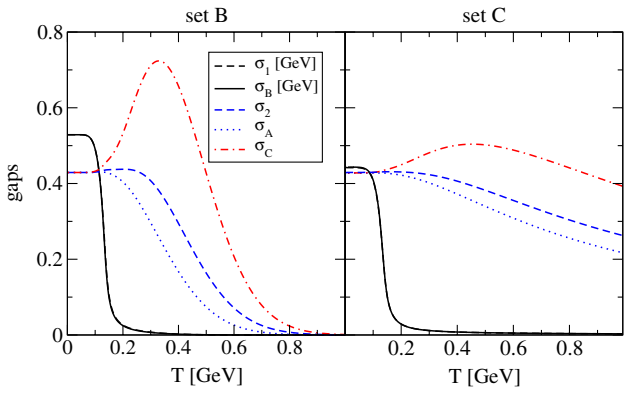

FIG. 1 (color online). We illustrate the effect of LSB in set B (left) and set C (right) at $\mu=0$. For simplicity, the system has been solved without PL.

reflection of the $R^3\times S^1$ structure of the spacetime manifold and was already observed in DSE separable model studies, e.g., Refs. [27,78]. At low temperatures, the thermal circle S^1 is large, and Lorentz symmetry is approximately valid. With the increase in the temperature, σ_A and σ_C split, the difference is starting to be pronounced around the phase transition as the gap equations form a coupled system. Namely, since around the phase transition the mass gap suffers a significant drop, this must be reflected in changes of the gaps σ_A and σ_C. We see that the particular behavior of the mean fields is "causal," governing the inequality $\sigma_A<\sigma_C$.

From Fig. 1, we conclude that the splitting is much stronger for set B; in the region $0.2\,{\rm GeV}\lesssim T\lesssim 0.6\,{\rm GeV}$, σ_C develops a pronounced peak, whereas σ_A monotonously descends. The value of σ_2 in the LS case can then be understood to provide a "mean value" between these two behaviors. The most distinct characteristic of the mean fields in set C is the finite value of σ_A and σ_C, referring to highly nonperturbative quarks even at $T\approx 1$ GeV.

The phase diagrams in this model for sets A, B, and C were presented in Ref. [48]. We are interested in the effect of the splitting of $\sigma_A-\sigma_C$ on the phase transition line, most notably on the position of the CEP.

The order parameter of chiral symmetry breaking is the quark condensate

$$\langle\bar{q}q\rangle=\frac{\partial\Omega_{\rm reg}}{\partial m}. \tag{41}$$

The pseudocritical temperature $T_{\rm c}$ in the crossover transition region is conveniently defined as in Ref. [48], with the temperature at which the chiral susceptibility $\chi=\partial\langle\bar{q}q\rangle/\partial m$ is maximal. For the first-order region, the point at which the chirally broken and chirally restored solution of the gap equation have the same value of the thermodynamic potential defines the transition point in the phase diagram. This way, a curve $T_c(\mu)$ in the $T-\mu$ plane is provided.

Even though the mass gap is practically identical in both setups, see Fig. 1, the quark condensate is also affected by σ_A and σ_C; thereby, some difference in the critical line is to be anticipated. However, we do not expect the actual change to be drastic, as the condensate is mostly driven by the value of the mass gap.

Figure 2 shows results for the phase diagrams of rank-2 models: set B and set C in both cases. Some general remarks are in order. First, the presence of the PL increases the pseudocritical temperature $T_c(0)$ in both models by ~50 MeV. This can be argued by a simple analytical formula provided by Ref. [48] and from the fact that the pure Yang–Mills (YM) sector provides a transition temperature of $T_0=0.27$ GeV [72]. Second, the first-order transition of the pure YM sector "pushes" the CEP closer to the T axes. Finally, the effect of the PL

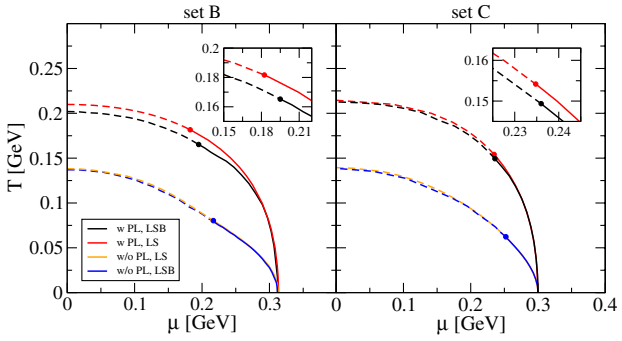

FIG. 2 (color online). Left (right) panel: phase diagrams for set B (set C) for cases with and without PL. With PL and LSB, the results are shown in black, while the results from Ref. [48] are repeated in red. Blue (orange) lines are results without PL and with (without) LSB. The dashed line denotes crossover, and the full line is the first-order transition.

is less significant once the temperature is sufficiently low. Critical lines of both cases, with and without PL, join at $T = 0$.

The explicit value of $T_c(0)$ is somewhat high, being around 0.2 GeV regardless of the model details, while lattice results for two flavors [79] provide a value of 0.17 GeV. This can be easily amended by rescaling the YM critical temperature T_0 as argued in Ref. [80]. Within nl-PNJL models, the effect of such a rescaling on the pseudocritical temperature $T_c(0)$ and on the width of the transition has been explored, e.g., in Refs. [49,50]. In Ref. [77], an account on the phase diagram in nl-PNJL, with rescaled T_0, can be found (see also Ref. [81]).

For set B, the critical lines, as given in left panel of Fig. 2, are changed only in the high-T, low-μ region. Specifically, we obtain a somewhat lower $T_c(0)$ for the LSB case, in accordance with the analytical estimate (34). The region around CEP is slightly altered, shifting the value of the CEP to lower T and higher μ for $\sim$20 MeV. We regard the critical lines for set C, on the right panel of Fig. 2, as almost identical, with the LSB curve being only a few MeV below the one reported in Ref. [48]. This is just a reflection of the results in the previous section, where, at least for $\mu = 0$, Fig. 1 explicitly shows that the $\sigma_A - \sigma_C$ splitting is much stronger for set B than for set C.

IV. FINITE TEMPERATURE MEAN-FIELD EQUATION OF STATE

In the following section, first, a brief summary of results found in Ref. [73] is highlighted in order to explain why thermodynamic instabilities are in general expected when one deals with covariant quark models. Technical steps are omitted for brevity. Moreover, we upgrade the study of the analytic structure of rank-1 models with a Gaussian regulator [24,25,29] to rank 2, revealing a crucial difference between these two models, needed for understanding the thermal behavior of the EoS. Finally, we analyze the difference of the EoS with and without LS.

A. Instability in covariant chiral quark models

The central quantity is the kinetic contribution to the thermodynamic potential (6). To understand the principle mechanism, it is sufficient to conjecture that the quark propagator has a series of P simple CCMPs. By standard residue analysis [73] in the case without the PL, one is then able to obtain

$$\begin{aligned}\Omega_{\rm kin} &= \Omega_{\rm zpt} - 4TN_fN_c\sum_{k=1}^{P}\int\frac{d^3p}{(2\pi)^3}\\ &\quad\times[\log(1+e^{-\beta\mathcal{E}_k})+\log(1+e^{-\beta\mathcal{E}_k^*})]\\ &= \Omega_{\rm zpt} - 4TN_fN_c\sum_{k=1}^{P}\int\frac{d^3p}{(2\pi)^3}\\ &\quad\times\log[1+2\ \cos(\beta\gamma_k)e^{-\beta\epsilon_k}+e^{-2\beta\epsilon_k}],\end{aligned}\tag{42}$$

where the notation $\mathcal{E}_k(\mathbf{p}) = \epsilon_k(\mathbf{p}) + i\gamma_k(\mathbf{p})$ for the CCMPs was used. They are given as

$$\epsilon_k(\mathbf{p}) = \frac{1}{\sqrt{2}}\left\{(m_k^R)^2 - (m_k^I)^2 + \mathbf{p}^2 + \sqrt{[(m_k^R)^2 - (m_k^I)^2 + \mathbf{p}^2]^2 + 4(m_k^R)^2(m_k^I)^2}\right\}^{1/2}\tag{43}$$

and

$$\begin{aligned}\gamma_k(\mathbf{p}) &= \frac{m_k^R m_k^I}{\epsilon_k(\mathbf{p})}\\ &= \frac{1}{\sqrt{2}}\left\{-(m_k^R)^2 + (m_k^I)^2 - \mathbf{p}^2 + \sqrt{[(m_k^R)^2 - (m_k^I)^2 + \mathbf{p}^2]^2 + 4(m_k^R)^2(m_k^I)^2}\right\}^{1/2},\end{aligned}\tag{44}$$

where m_k^R and m_k^I are real and imaginary parts of complex masses, respectively. In general, they are functions of the mean fields

$$m_k^R = m_k^R(\sigma_A,\sigma_B,\sigma_C), \qquad m_k^I = m_k^I(\sigma_A,\sigma_B,\sigma_C).\tag{45}$$

The quantity $\Omega_{\rm zpt}$ represents the zero-point energy. With the combined logarithms in the second equality, it is easily observed that a nonzero value of at least one γ_k leads to an oscillating EoS. Namely, if the oscillations are expected in the confining, low-T domain, one can perform an expansion in $m_k^R/T \gg 1$ of the thermal part in Eq. (42). If, in addition, one assumes that $m_k^I \ll m_k^R$, then

$$\Omega_{\rm kin} \simeq \Omega_{\rm zpt} - 4N_f N_c T^4 \sum_{k=1}^{P}\left[2\,\cos\left(\frac{m_k^I}{T}\right)\left(\frac{m_k^R}{2\pi T}\right)^{3/2} e^{-m_k^R/T} + \left(\frac{m_k^R}{4\pi T}\right)^{3/2} e^{-2m_k^R/T}\right], \tag{46}$$

which is a generalization of the low-temperature expansion [64] for complex masses.

Including the effect of the PL, i.e., performing a Matsubara sum in Eq. (21), gives

$$\begin{aligned}\Omega_{\rm kin} = \Omega_{\rm zpt} - 4N_f T \sum_{k=1}^{P}\int \frac{d^3p}{(2\pi)^3}\,\log\{1 + 6\Phi[(e^{-\beta\epsilon_k} + e^{-5\beta\epsilon_k})\,\cos(\beta\gamma_k) \\ + (e^{-2\beta\epsilon_k} + e^{-4\beta\epsilon_k})\,\cos(2\beta\gamma_k)] \\ + 9\Phi^2[e^{-2\beta\epsilon_k} + e^{-4\beta\epsilon_k} + 2e^{-2\beta\epsilon_k}\,\cos(\beta\gamma_k)] + 2e^{-3\beta\epsilon_k}\,\cos(3\beta\gamma_k) + e^{-6\beta\epsilon_k}\},\end{aligned} \tag{47}$$

reflecting the stabilization mechanism by the PL: in the confining phase, $\Phi \approx 0$, and the oscillating terms are significantly suppressed. This can be explicitly seen in the low-T expansion of Eq. (47),

$$\begin{aligned}\Omega_{\rm kin} \simeq \Omega_{\rm zpt} - 4N_f T^4 \sum_{k=1}^{P}\Bigg\{6\Phi\,\cos\left(\frac{m_k^I}{T}\right)\left[\left(\frac{m_k^R}{2\pi T}\right)^{3/2} e^{-m_k^R/T} + \left(\frac{m_k^R}{10\pi T}\right)^{3/2} e^{-5m_k^R/T}\right] \\ + 6\Phi\,\cos\left(\frac{2m_k^I}{T}\right)\left[\left(\frac{m_k^R}{4\pi T}\right)^{3/2} e^{-2m_k^R/T} + \left(\frac{m_k^R}{8\pi T}\right)^{3/2} e^{-4m_k^R/T}\right] \\ + 9\Phi^2\left[\left(\frac{m_k^R}{4\pi T}\right)^{3/2} e^{-2m_k^R/T} + \left(\frac{m_k^R}{8\pi T}\right)^{3/2} e^{-4m_k^R/T} + 2\,\cos\left(\frac{m_k^I}{T}\right)\left(\frac{m_k^R}{4\pi T}\right)^{3/2} e^{-2m_k^R/T}\right] \\ + 2\,\cos\left(\frac{3m_k^I}{T}\right)\left(\frac{m_k^R}{6\pi T}\right)^{3/2} e^{-3m_k^R/T} + \left(\frac{m_k^R}{12\pi T}\right)^{3/2} e^{-6m_k^R/T}\Bigg\}.\end{aligned} \tag{48}$$

B. Overcritical vs undercritical mass gaps

In the last subsection, we have argued that oscillations may appear in the EoS if at least one γ_k is complex. Now, we will make the preparatory analysis in order to be able to discuss in which temperature region that occurs.

To understand the connection between the oscillations and the mass gap σ_1, one traces singularities as functions of σ_1. The salient features will be presented for Gaussian regulators and in the chiral limit. We will also restrict the analysis to the lowest-lying poles as they carry all the essential properties in the temperature range that is discussed.

For a rank-1 Gaussian model, a value of $\sigma_1 > \sigma_1^c$, where $\sigma_1^c = \Lambda_0/(\sqrt{2e})$ gives only complex poles in the propagator, while $\sigma_1 < \sigma_1^c$ gives also a pair of real poles. In set A, the vacuum value is overcritical, i.e., $\sigma_1 > \sigma_1^c$; thus, all the poles are complex, and the oscillations are present in the $T \lesssim T_c$ region. More concretely, in the chiral limit, we have $\sigma_1 = 0.402$ GeV and $\sigma_1^c = 0.322$ GeV. ILM models usually support weaker interaction strengths, as is, e.g., the case for the specific parameters discussed here; see Table I. This typically leads to undercritical gaps; for parameters given in Table I in the chiral limit, we have $\sigma_1 = 0.215$ GeV, and $\sigma_1^c = 0.387$ GeV.

For rank 2, we facilitate the analysis further by considering the case $\Lambda_0 = \Lambda_1$. With $\sigma_2 = 0$, two real poles exist, as shown on Fig. 3. Any $\sigma_2 > 0$ brings an extra pole σ_1/σ_2 from infinity. As σ_2 increases, this singularity

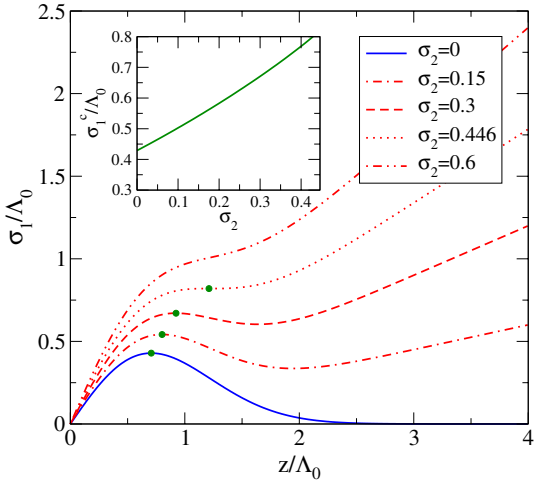

FIG. 3 (color online). The structure of only real singularities z as functions of the mass gap σ_1 are shown for the Gaussian regulators of a rank-2 model. Setting $\sigma_2 = 0$ leads back to the rank-1 model given by the blue curve. Nonzero values of σ_2 then give a family of red curves, where the green dot gives $\sigma_1^c(\sigma_2)$ (see the text). The full function $\sigma_1^c(\sigma_2)$ is obtained numerically and shown in the inset.

in turn coalesces with the first two at $\sigma_2 = \sigma_2^c = 2/e^{3/2} \simeq 0.446$, after which point only one real singularity is present for all values of σ_1. At the same time, the threshold σ_1^c rises as a function of σ_2, until it reaches

$$\sigma_1^c(\sigma_2^c) = \frac{\Lambda_0}{\sqrt{2}}\left(\frac{3}{e}\right)^{3/2}, \tag{49}$$

as shown by the green line in the inset of Fig. 3. The outcome is that in rank 2 it is easier for the physical mass gap to be undercritical. A concrete calculation for set B with $\Lambda_0 = \Lambda_1$ yields $\sigma_1 = 0.497$ GeV, $\sigma_2 = 0.430$, so that $\sigma_1^c(0.430) = 0.652$ GeV, confirming that indeed the gap is undercritical.

C. Entropy density

At this point, we are ready to analyze the resulting mean field EoS at finite temperature as obtained from

$$p = -\Omega_{\text{reg}}. \tag{50}$$

It is particularly useful to examine the entropy density

$$s = \frac{dp}{dT}. \tag{51}$$

Being a derivative of the pressure (50) with respect to the temperature, the entropy density will make any possible unphysical behavior most transparent, such as the oscillations found in Ref. [73], and therefore be suitable for selecting a preferable model.

If the gap is overcritical, oscillations shall be present in Gaussian models, the complex exponential of the regulators giving rise to an infinite number of poles. It is more involved to extract an analytic structure of set C, containing cuts as well as poles, so we restrict our discussion to the numerical results. In all cases, the PL will play an important role. The results in Fig. 4 are given for all three different regulators and for the ILM model and scaled to the massless Stefan–Boltzmann (SB) value. Whereas a smooth, monotonous rise in the entropy is expected as the quark degrees of freedom are liberated, nonphysical oscillations are present for all three regulators, as anticipated in the first subsection.

To underline the fact that complex singularities are crucial for oscillations, it is useful to consider the comparison of the entropy in set A (blue) and in the ILM (green, dotted curve). The low-T region is shown in the inset on the left panel. There, it is clearly visible that the effect of the CCMPs is given in the low-temperature region for set A

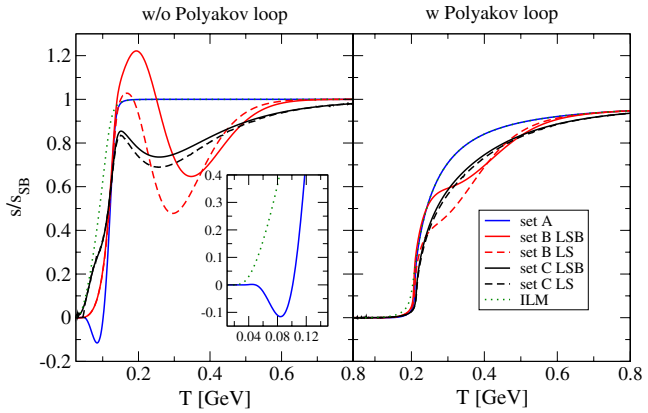

FIG. 4 (color online). Scaled entropy density as a function of temperature. The left panel is without PL, while the right panel includes the PL. Notice the temperature mismatch in the oscillations for set A vs sets B and C. Since the gap in the ILM model is undercritical, there are no oscillations in the low-T phase even in the case without the PL, as shown in the inset.

but not for the ILM. The reason is that, since the mass gap in the latter case is undercritical, the lowest-lying singularities, which dominate the entropy at low T, are real; see also Fig. 3.

Furthermore, the SB limit is well saturated already at $T \gtrsim T_c$ when the system is not coupled to the PL; see the blue curve on the left panel of Fig. 4. A significant change in the onset is achieved when coupling to the PL, but this should be attributed to the fact that the PL potential $\mathcal{U}(\Phi)$ is fitted to lattice data for the pressure of pure glue.

For set B, which in addition has the WFR channel, the mass gap becomes undercritical (see Fig. 3), so that the behavior of entropy is monotonous at $T \lesssim T_c$ as observed by the red curve in the left panel of Fig. 4. In contrast, here, the oscillatory behavior is present exclusively at $T \gtrsim T_c$. Because of the analysis in the first subsection, we may again attribute this behavior to complex singularities. But, since σ_B is drastically reduced, they are linked to the analytical properties of the WFR term.

To confirm this conjecture, it is sufficient to look for complex poles for set B in a idealized scenario in which the mass gap is zero and where $A(p^2) = C(p^2)$. If we are able to prove that there are poles in the degenerate quark propagator (7) with $B(p^2) = 0$, besides the massless one, then we can use Eq. (42) to again argue that they are responsible for oscillations seen in Fig. 4. For set B, one can show that the condition $A(-\mathcal{E}_k^2) = 0$, is fulfilled with

$$\epsilon_k(\mathbf{p}) = \frac{\Lambda_1}{\sqrt{2}}\left[\sqrt{\left(\frac{\mathbf{p}^2}{\Lambda_1^2} - \log\sigma_2\right)^2 + (2k+1)^2\pi^2} + \frac{\mathbf{p}^2}{\Lambda_1^2} - \log\sigma_2\right]^{1/2}, \qquad \gamma_k(\mathbf{p}) = \frac{(2k+1)\pi}{2\epsilon_k(\mathbf{p})}\Lambda_1^2, \tag{52}$$

where $k \in \mathbb{Z}$ and for set C

$$\mathcal{E}_k(\mathbf{p}) = \Lambda_1 \left[1 + \frac{\mathbf{p}^2}{\Lambda_1^2} - (\alpha_z + \sigma_2 + \alpha_z \sigma_2)^{2/5} e^{\frac{2\pi k i}{5}} \right]^{1/2}, \quad (53)$$

with $k = 0, 1, \ldots, 4$. Interestingly, in set B, even though the number of poles is infinite, we can still find a clear hierarchy. For example, if $\sigma_2 = 1$, then

$$m_k^R = m_k^I = \Lambda_1 \sqrt{\frac{\pi}{2} + k\pi}.$$

Notice also that, as $\sigma_2 \to 0$, for set B, we find $\epsilon_k(\mathbf{p}) \to \infty$ and $\gamma_k(\mathbf{p}) \to 0$, ensuring that, in the high-temperature range where $\sigma_2 \to 0$, one is left with the usual massless singularity. The analogous formula for set C (53) is valid only when $\sigma_2 \neq 0$: the limiting case is provided by going back to the original formula $p^2 A^2(p^2) = 0$. More importantly, as Eqs. (52) and (53) are double poles, the SB limit is eventually exceeded, as demonstrated by the red curve in Fig. 4. This unsatisfactory result is readily improved with the lattice-adjusted set C parametrization; the oscillation is somewhat reduced, giving an entropy within the SB bound, over the whole temperature range.

Introducing the PL to the system leads to a dramatically improved behavior. As the right panel of Fig. 4 indicates, there is a smooth rise in the entropy for set A, in accordance with Eq. (47). The PL is very successful in taming the oscillations in a theory with CCMPs, as its value is zero in the low-temperature, confined phase. As the confinement transition is coincident with the chiral one, the only poles that the PL are able to strongly suppress are the ones present before the chiral transition. Therefore, the oscillation in set B, due to the double poles, is still present, albeit largely reduced, owing to the fact that Φ is still less than unity in that region. For set C, the oscillation was smaller to begin with, so when the PL smooths that out, all that is left is again a monotonous rise, as observed by the black curve in the right panel of Fig. 4. The same effect is visible in a recent calculation in $N_f = 2 + 1$ nl-PNJL [82].

D. Influence of Lorentz symmetry breaking

The influence of LSB is minor, being somewhat stronger for set B. In particular, the two black curves in the right panel of Fig. 4 for entropy density in set C with PL are almost identical, whereas for set B, LSB can lead even to a 20% increase for $T \gtrsim T_c$. A qualitative understanding of this effect can be achieved from the quasiparticle picture given by Eq. (26). The particular value of the entropy could be seen as the interplay of the two effects: increasing m_{qp} decreases the entropy ("loss" term), while increasing v_{qp} increases the entropy ("gain" term). A ratio of the masses and the velocities for the LSB and the LS case yields

$$\frac{v_{\mathrm{qp}}^{\mathrm{LSB}}}{v_{\mathrm{qp}}^{\mathrm{LS}}} = \frac{1+\sigma_A}{1+\sigma_C}, \qquad \frac{m_{\mathrm{qp}}^{\mathrm{LSB}}}{m_{\mathrm{qp}}^{\mathrm{LS}}} = \frac{1+\sigma_2}{1+\sigma_C}, \quad (54)$$

where we have used that $v_{\mathrm{qp}}^{\mathrm{LS}} = 1$, and $\sigma_1 \simeq \sigma_B$, which is well fulfilled in our case; see Fig. 1. From Fig. 1, we also deduce that $\sigma_2 > \sigma_A$; thus,

$$\frac{m_{\mathrm{qp}}^{\mathrm{LSB}}}{m_{\mathrm{qp}}^{\mathrm{LS}}} : \frac{v_{\mathrm{qp}}^{\mathrm{LSB}}}{v_{\mathrm{qp}}^{\mathrm{LS}}} = \frac{1+\sigma_2}{1+\sigma_A} > 1, \quad (55)$$

which can be interpreted to mean that the loss term in the entropy density is less significantly affected by LSB than the gain term, providing a net increase of the entropy density.

V. MESON DECAY WIDTHS AT FINITE TEMPERATURE

At this point, we discuss the thermal behavior of mesonic degrees of freedom. In a local NJL setup, this has been thoroughly studied. We expect that nonlocal interactions might induce new features particularly into the picture of meson dissociation in the plasma. The aim is to deduce qualitative influence of nonlocal interactions on the aspect of Mott physics such as resonance broadening and also to discuss the effects of the WFR channel. Since the explicit calculations are performed with LSB, all the mean fields are denoted as $\sigma_{A,B,C}$.

The in-medium features of correlations are encoded in the meson polarization function [27,78,83,84]

$$\Pi_M(\nu_m, |\mathbf{q}|) = \frac{8N_c}{3} T \sum_{n=-\infty}^{\infty} \int \frac{d^3p}{(2\pi)^3} \mathrm{tr}_C \left[g^2(\tilde{p}_n^2) \times \frac{K_M(\tilde{\omega}_n^2, \mathbf{p}^2, \nu_m^2, \mathbf{q}^2)}{\mathcal{D}((\tilde{\omega}_n^+)^2, (\mathbf{p}^+)^2) \mathcal{D}((\tilde{\omega}_n^-)^2, (\mathbf{p}^-)^2)} \right], \quad (56)$$

with

$$K_M(\tilde{\omega}_n^2, \mathbf{p}^2, \nu_m^2, \mathbf{q}^2) = (\tilde{\omega}_n^+ \tilde{\omega}_n^-) C((\tilde{p}_n^+)^2) C((\tilde{p}_n^-)^2) + (\mathbf{p}^+ \cdot \mathbf{p}^-) A((\tilde{p}_n^+)^2) A((\tilde{p}_n^-)^2) \pm B((\tilde{p}_n^+)^2) B((\tilde{p}_n^-)^2), \quad (57)$$

generalized in order to include effects of LSB. We use the subscript M for specifying the meson $M = \pi, \sigma$ and denote the meson 4-momentum as $q_m = (\nu_m, \mathbf{q})$, where $\nu_m = 2m\pi T$ are the bosonic Matsubara frequencies. Furthermore, $\tilde{p}_n^{\pm} = (\tilde{\omega}_n^{\pm}, \mathbf{p}^{\pm})$, with $\tilde{\omega}_n^{\pm} = \tilde{\omega}_n \pm \nu_m/2$, and $\mathbf{p}^{\pm} = \mathbf{p} \pm \mathbf{q}/2$ and

$$\mathcal{D}(-z^2, \mathbf{p}^2) = \mathbf{p}^2 A^2(-z^2 + \mathbf{p}^2) - z^2 C^2(-z^2 + \mathbf{p}^2) + B^2(-z^2 + \mathbf{p}^2). \quad (58)$$

It will be crucial to note that Eq. (56) is valid only for sets A–C. The polarization function in the ILM follows by making a replacement,

$$g^2(\tilde{p}_n^2) \to r^2((\tilde{p}_n^+)^2) r^2((\tilde{p}_n^-)^2), \tag{59}$$

in the first term after the square bracket in Eq. (56). The regulator in the $B(p^2)$ function in the propagator is altered accordingly, i.e., so that $g(p^2) \to r^2(p^2)$.

A. Meson widths

The width is obtained by renormalizing the meson propagator. For simplicity, if we take the vacuum propagator in Euclidean space and expand it around $q^2 = -m_M^2$,

$$\Delta(q^2) = \frac{1}{-\frac{1}{G_S} + \Pi_M(q^2)} \to \frac{g_{M\bar{q}q}^2}{q^2 + m_M^2 + i\Gamma_M m_M}, \tag{60}$$

where Γ_M is the meson width

$$\Gamma_M = g_{M\bar{q}q}^2 \frac{\mathrm{Im}(\Pi_M)}{m_M} \tag{61}$$

and $g_{M\bar{q}q}$ is the effective quark-meson coupling, or the meson wave function renormalization

$$g_{M\bar{q}q}^2 = \left[\frac{\partial \mathrm{Re}(\Pi_M)}{\partial q^2}\right]^{-1}_{q^2=-m_M^2}. \tag{62}$$

We will obtain $\mathrm{Im}(\Pi_M)$ as a function of the meson energy, denoted by q_0, at rest $\mathbf{q} = 0$. In doing so, we will use several simplifications and approximations, to be stated precisely in the following.

First of all, it is known in the literature [34,83,85] that an elaborate analytic continuation of the polarization loop is possible that does not lead to thresholds in the case the singularities of the quark propagator are complex. In other words, if the quark propagator has only complex singularities, the meson is stable.

As we have shown, some of the models that we study here, like set A, have such property in the vacuum. On the other hand, models like set B and the ILM have also real singularities in the vacuum. Taking the parameters given in Table I, their values, denoted as m_L, are $m_L = 0.508$ GeV for set B and $m_L = 0.331$ GeV for the ILM. So, in principle, if the condition for the kinematic threshold is satisfied, i.e., if $m_M > 2m_L$, the meson must be unstable. It turns out that, for set B and the ILM, this is not the case—in other words, pion and sigma mesons are stable in the vacuum, and the explicit values are collected in Table II.

Proceeding to finite T, it is possible for mesons to develop finite imaginary parts if some of kinematic thresholds become allowed. A complete discussion requires mapping the behavior of the singularities as a function of temperature, which in turn requires mapping them as a function of the mean fields $\sigma_{A,B,C}$. In the case of rank-1 models, like set A and the ILM, we have a single mean field σ_B. Then, the thermal dependence of the lowest-lying singularities can be numerically mapped and are shown on Fig. 5 for set A in the chiral limit, where singularities are complex in vacuum. As the temperature increases, σ_B decreases— when it reduces below σ_B^c, we have real singularities, denoted as m_L and m_H. The singularity m_H

TABLE II. For sets A–C, and the ILM, the table collects vacuum values of the mass gaps σ_B, the critical values σ_B^c at which the physical continuum moves from the real axes, together with the respective temperature T_{cont} where this happens. We also provide the Mott temperatures for π and σ mesons. Note that, for set A, the physical mass gap is overcritical, while for set B and the ILM, it is undercritical. For set C, the imaginary part develops continuously from the current quark mass m. Therefore, the continuum is present in the ILM and sets B and C already at $T = 0$. The table also gives the actual values for the lowest real singularities in the vacuum, denoted by m_L. Furthermore, we provide the vacuum values of the masses and the quark-pion couplings.

	Set A	Set B	Set C	ILM
σ_B [GeV]	0.424	0.429	0.442	0.284
σ_B^c [GeV]	0.317	0.557	0.0	0.391
m_L [GeV]	⋯	0.508	⋯	0.330
T_{cont} [GeV]	0.208	0	0	0
T_{Mott}^{π} [GeV]	0.21	0.21	0.22	0.20
$T_{\mathrm{Mott}}^{\sigma}$ [GeV]	0.21	0.21	0.21	0.20
m_π [GeV]	0.14	0.14	0.14	0.14
m_σ [GeV]	0.68	0.63	0.56	0.4
$g_{\pi\bar{q}q}$	4.62	5.74	4.74	2.47

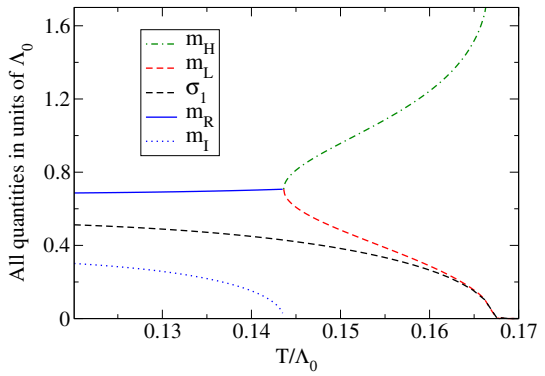

FIG. 5 (color online). Temperature dependence of lowest singularities for set A in the chiral limit and without the Polyakov loop. The full blue and dotted blue lines are the real (m_R) and imaginary (m_I) parts of the lowest lying singularity, respectively. Beyond a certain temperature given by the condition $\sigma_B(T) = \sigma_B^c$, these poles join on the real axis to form two real poles, m_L given by the red dashed line and m_H given by the green dashed-dotted line. The mass gap σ_B is also shown to illustrate how, as $T \to T_c$, m_L approaches σ_B.

becomes very heavy as we approach chiral restoration—therefore, the meson will not decay into the state m_H. On the contrary, m_L becomes the massless, chiral singularity; therefore, we consider the decay of the meson to m_L.

For set B and set C models, where additional mean fields are present, we do not map the singularities as functions of the mean fields, although this is, in principle, possible. Based on the previous analysis in the vacuum, and for rank-1 models also at finite temperature, we anticipate the following idealized scenario. At low temperatures, all the singularities in the models are either complex or real, but in both cases, they are at least of the order of the scale of the regulators $f(p^2)$ and $g(p^2)$, which is out of reach as a continuum threshold. Increasing the temperature, the mass gap drops. This forces one pole to proceed to $m_{\rm qp}$ as defined in Eq. (26) and then to the origin in the complex plane becoming the physical, current quark mass for very high temperatures. See Fig. 5 for an explicit example in the case of rank 1. The other auxiliary states have either complex masses or very heavy real masses. In either case, it is important to realize that they will not contribute to the imaginary part. In total, the imaginary part, and therefore nonzero width, will be generated by the decay of the meson to the singularity that continuously evolves to the current quark mass.

Now, we can calculate the imaginary part by applying the $i\epsilon$ prescription for the mass $m_{\rm qp}$,

$$\begin{aligned}\mathrm{Im}[\Pi_M(-iq_0,0)] = \frac{1}{2i}[&\Pi_M(-i(q_0+i\epsilon),0)\\ &-\Pi_M(-i(q_0-i\epsilon),0)],\end{aligned} \tag{63}$$

where the bosonic Matsubara frequencies were analytically continued to $i\nu_m \to q_0$ and where the imaginary part will be calculated at $\mathbf{q}=0$. The master formula for performing the summation over the fermionic Matsubara frequencies, as well as the detailed derivation of the imaginary part of Eq. (56), are collected in the Appendix A. Here, we quote the final result for sets A–C,

$$\begin{aligned}\mathrm{Im}[\Pi_M(-iq_0,0)] = &\frac{d_q}{16\pi}[1-n_+^\Phi(q_0/2)-n_-^\Phi(q_0/2)]\\ &\times\sqrt{1-\left(\frac{2m_{\rm qp}}{q_0}\right)^2}\,g^2\left(\frac{q_0^2}{4}-m_{\rm qp}^2\right)\\ &\times\frac{K_M\left(0,\frac{q_0^2}{4}-m_{\rm qp}^2,-q_0^2,0\right)}{\left[\mathcal{D}'\left(-\frac{q_0^2}{4},\frac{q_0^2}{4}-m_{\rm qp}^2\right)\right]^2}\\ &\times\theta\left(\frac{q_0}{2}-m_{\rm qp}\right),\end{aligned} \tag{64}$$

with $\mathcal{D}'$ defined by Eq. (A4). The square bracket in the first line of Eq. (64) defines the Pauli blocking term, with $n_\pm^\Phi(z)$ being the generalized occupation number for fermions in the presence of the Polyakov loop Φ and its conjugate $\bar\Phi$,

$$n_\pm^\Phi(z)=\frac{\bar\Phi e^{-\beta(z\mp\mu)}+2\Phi e^{-2\beta(z\mp\mu)}+e^{-3\beta(z\mp\mu)}}{1+3\bar\Phi e^{-\beta(z\mp\mu)}+3\Phi e^{-2\beta(z\mp\mu)}+e^{-3\beta(z\mp\mu)}}. \tag{65}$$

The imaginary part of the polarization loop $\mathrm{Im}(\Pi_M)$ for the ILM follows by making the replacement (59) while taking into account that the quasiparticle energies are dictated by energy conservation, see the δ function in Eq. (A7), yielding

$$g^2\left(\frac{q_0^2}{4}-m_{\rm qp}^2\right)\to r^4(-m_{\rm qp}^2). \tag{66}$$

Notice that as the quasiparticle mass goes to the current quark mass; in the ILM model, this prefactor $r^4(-m_{\rm qp}^2)\to 1$. On the other hand, in sets A–C, ignoring the small current mass, we will still be left with $g^2(q_0^2/4)$. This might have a significant impact in the high-T phase, depending on the value of q_0.

It is interesting to discuss the local limit, where we obtain

$$K_M \simeq \frac{q_0^2}{4}C_0^2+\left(\frac{q_0^2}{4}-m_{\rm qp}^2\right)A_0^2\pm m_{\rm qp}^2,\qquad \mathcal{D}'\simeq C_0^2. \tag{67}$$

Furthemore, by taking A_0, $C_0\to 1$, we reproduce the local NJL result [86]

$$\begin{aligned}\mathrm{Im}[\Pi_M(-iq_0,0)]\to\frac{d_q}{16\pi}[&1-n_+^\Phi(q_0/2)\\ &-n_-^\Phi(q_0/2)]\sqrt{1-\left(\frac{2m_{\rm qp}}{q_0}\right)^2}\\ &\times\left[\frac{q_0^2}{4}-m_{\rm qp}^2\pm m_{\rm qp}^2\right]\theta\left(\frac{q_0}{2}-m_{\rm qp}\right).\end{aligned} \tag{68}$$

On the other hand, by using Eq. (67), in the chiral limit, we obtain

$$\frac{K_M}{(\mathcal{D}')^2}\to\frac{q_0^2}{4}\frac{1}{C_0^2}(1+v_{\rm qp}^2). \tag{69}$$

This result shows that introducing WFR can significantly reduce the imaginary part. In addition, if LSB by the medium is acknowledged, owing to the fact that $v_{\rm qp}<1$, the imaginary part will be even more reduced.

As we expect degeneracy of the meson states above the chiral transition temperature, in practice, it will be sufficient to consider the pion width. To do that, we need two more ingredients: q_0 and $g_{\pi\bar qq}$. In local NJL, see e.g., Ref. [86], and 3D nl-NJL studies [23], it is shown that $g_{\pi\bar qq}$ is a slowly varying function of the temperature. Actually, for $g_{\pi\bar qq}$, this can be naturally understood from the quark-level Goldberger–Treiman relation $g_{\pi\bar qq}\sim m_{\rm qp}/f_\pi$, where f_π is the pion decay constant. Up to the temperatures close to chiral restoration, both $m_{\rm qp}$ and f_π are constant, while around and after T_c, they both get monotonously reduced.

Hence, to get an idea of the pion width also in a covariant (four-dimensional) nl-PNJL setup, we make a rough approximation by replacing the thermal dependence of the quark-pion coupling $g_{\pi\bar{q}q}$ by its vacuum value. The calculated values for all the models considered in this work are collected in Table II.

B. Meson masses

To calculate the width, we still need q_0, which should, in principle, be given by the dynamical, pole mass m_M^{pole}, obtained from its Bethe–Salpeter equation at zero meson momentum $\mathbf{q} = 0$:

$$1 - G_S \Pi_M(-im_M^{\text{pole}}, 0) = 0. \tag{70}$$

While such calculations are straightforward in local NJL models, the covariant approach presents technical difficulties. Namely, a complete analysis requires performing Matsubara summation analytically. Since the polarization loop contains a pair of quark propagators, via residue calculus, this will, in principle, lead to a double summation over all the singularities present in the propagator, requiring that their behavior first needs to be traced as a function of the mean fields $\sigma_{A,B,C}$. Note that this is significantly more involved than the imaginary part since here we need the information on singularities in the low- as well as in the high-T regimes, whereas, for the imaginary part, we needed only one singularity in the high-T regime.

Since the aim of the present section is the qualitative analysis of the meson widths obtained within models, for q_0, we have chosen to use by hand the meson screening masses [27,78,83,84] m_M^{spat} given by solving the equation

$$1 - G_S \Pi_M(0, -im_M^{\text{spat}}) = 0. \tag{71}$$

This simplification is supported by a calculation in local NJL models [87,88], where a careful comparison of both screening and pole masses lead to the following conclusion: at low temperatures, below the chiral restoration temperature, the screening masses closely follow the dynamical ones. However, at temperatures above the chiral restoration, screening masses were found to be somewhat higher in value. It should be emphasized that both the screening and the pole masses were found to follow the expected pattern of chiral symmetry breaking and restoration.

C. Discussion of the results

In Fig. 6, we plot the sigma and pion spatial masses, as calculated from Eq. (71). Besides the spatial meson masses, it is instructive to show the "continuum" states defined by $2m_{\text{qp}}$, where m_{qp} is given by Eq. (26). Strictly speaking, these states need not be present as actual singularities of the quark propagator up to some high temperature, as was previously discussed.

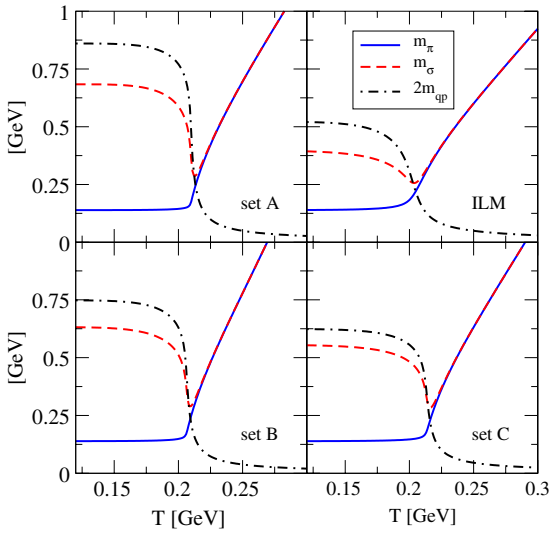

FIG. 6 (color online). The panels display screening masses for π and σ mesons for different sets. The results for sets B and C are only for the LSB case.

Returning to our canonical example in set A, the continuum states are developed only after the temperature at which $\sigma_B = \sigma_B^c$. For finite current quark mass, this happens at $T_{\text{cont}} = 0.208$ GeV. Let us now define the Mott temperatures by

$$m_M^{\text{spat}}(T_M^{\text{Mott}}) = 2m_{\text{qp}}(T_M^{\text{Mott}}).$$

Now, from Fig. 6, we observe that the Mott temperatures for both π and σ are higher than T_{cont}, i.e., $T_\pi^{\text{Mott}} = 0.213$ GeV, $T_\sigma^{\text{Mott}} = 0.212$ GeV, thus providing a picture in which the continuum of states should be first realized in the singularities of the quark propagator, so that the meson decay can happen only at higher temperatures. This is also the situation in all other models, i.e., $T_M^{\text{Mott}} > T_{\text{cont}}$ for sets B and C and the ILM. The complete set of values of Mott and continuum temperatures is collected in Table II.

We see that introducing WFR lowers the continuum according to the Eq. (26). Also, the σ meson mass is reduced, which one would naively agree to from the PNJL setting in which $m_\sigma \simeq 2m_{\text{qp}}$. The meson screening masses are joining at the chiral restoration temperature and tend to rise steeply beyond that point, approaching 1 GeV already around $T \simeq 0.3$ GeV, with the steepest rise for set B. The results for the ILM model single out because of its small mass gap, which in turn leads to a smoother transition into the chirally restored phase. As a further consequence, the sigma meson mass is almost twice reduced in the vacuum.

We calculate the widths by using spatial masses in Eq. (61) and in Eq. (64) by replacing $q_0 \to m_M^{\text{spat}}$, instead of the more accepted m_M^{pole}. This certainly introduces an error in our calculation, but since the qualitative behavior of both spatial and dynamical masses is the same, it will nevertheless provide a valuable study. In that sense, our results will be best seen as a study of the thermal

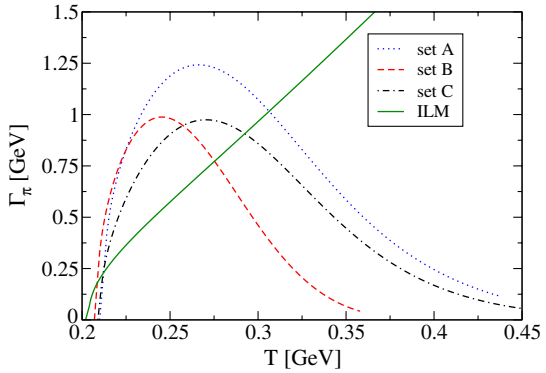

FIG. 7 (color online). The figure displays the approximate pion widths calculated from Eqs. (61) for sets A–C and the ILM.

dependence of the imaginary part of the polarization loop. Namely, instead of using a phenomenological fitting function for the mass as a function of the temperature, we employ the calculated screening masses. Then, since the width and the imaginary part are proportional, the *convention* for calculating the width itself is motivated by the fact that we would like to interpret our results physically.

Figure 7 shows the main result of this section. For sets A–C, inspired by the separable DSE calculation, the widths follow a generic pattern. In the low-temperature region, we find a steep rise, mostly due to the meson mass itself; see, e.g., the local and the chiral limit (69), at which one has a quadratic dependence on the meson mass in the imaginary part of the polarization loop, giving a linear slope for the width; see Eq. (61). But, since in the nonlocal models, the complete imaginary part, and therefore the width, is multiplied by the regulator, it is this factor that dictates the high-temperature behavior. Namely, as $g(p^2)$ is a rapidly decreasing function of momenta [see Eqs. (10)–(12)], and because for sets A–C the argument is a rising function of the temperature, it eventually overwhelms the quadratic dependence and provides a characteristic decrease in the width. Therefore, in the high-temperature phase, the width drops to zero. The quantitative result shown in Fig. 7 might be somewhat exaggerated due to the fact that the screening masses steeply rise with the temperature, making the decline of Γ_π more dramatic. Nevertheless, the qualitative behavior should be considered as generic to this class of models. In that regard, let us also comment on the fact that, as announced in the previous subsection, the width overall gets somewhat reduced when the WFR channel is introduced. This is demonstrated by the dashed, red, and dashed-dotted, black curves in Fig. 7.

Concentrating on the ILM calculation of the width, the result we obtain is completely different: because of the fact that the regulator in this case has a different momentum dependence in the polarization loop, see Eqs. (59) and (66), there is no dependence on the meson mass in the regulator, and its effect at high temperatures is highly suppressed. This results in a monotonous rise of Γ_π, shown by the full green curve, in the low- as well as in the high-temperature regions.

VI. CONCLUSIONS

In this work, we have discussed a class of nonlocal Polyakov–Nambu–Jona-Lasinio models which are suitably adjusted to model the behavior of the quark propagator in the vacuum as determined in lattice QCD simulations. These are extrapolated to finite T and μ whereby the new element of medium induced Lorentz symmetry breaking is introduced. In Sec. III, we have examined the influence of this term on the phase diagram, in the mean-field approximation. While LSB provides a significant difference in the wave function renormalization channel mean fields after T_c, we conclude the critical properties and the EoS do not change appreciably. We find, in general, that models with WFR tend to slightly lower the position of the CEP on the critical line. Complementary to numerical results, a thorough analytic study of the critical behavior in the vacuum and in the medium was given. Where possible, analytical limits to the local Polyakov–Nambu–Jona-Lasinio model were also given. While these are only estimates, it might be interesting to also examine a nontrivial WFR in a complete numerical setup of the local Polyakov–Nambu–Jona-Lasinio model.

In Sec. IV, we have calculated the EoS, concluding that for a wide class of nl-NJL models the EoS is oscillatory. We have demonstrated that, in contrast to rank-1 models with Gaussian regulator, for rank-2 models with Gaussian regulators, the mass gap is undercritical, thus giving a mismatch in the temperature at which the oscillations in the EoS occur. While for rank 1 they occur in the chirally broken phase, in rank 2, they occur in the chirally restored phase. For Lorentzian regulators, as in set C, we have found that the oscillations are also present, but somewhat less drastic. Such oscillations violate general thermodynamic criteria for the stability of the system and are not observed in lattice calculations. We have found that an improvement of the gluon sector, e.g., in the form of the Polyakov loop, significantly improves the thermodynamics. Nevertheless, since the Polyakov loop is finite in the high-temperature phase, the oscillations in rank-2 models are only reduced.

In Sec. V, we have presented a detailed derivation and a discussion of the widths in the covariant version of nonlocal models. We emphasize that the latter was completely absent from the literature, although the model itself has been present in the community for more than two decades. The basic problem is the covariance of the approach. More precisely, the fact that it is defined in Euclidean space makes "Minkowski quantities" like the dynamical meson masses and widths, difficult to obtain. Since we do not claim that we have solved this hard problem[3], the main drawback being that we have not

[3]A first step in solving it would be to map the analytic structure of the quark propagator in the complex plane. This is a highly nontrivial task, addressed only very recently [89–91].

calculated the dynamical pole masses but the spatial ones, we are nevertheless of the opinion that the results that we do display are still interesting to the community, as they bear a qualitative significance.

Thus, given the roughness of our approximations, we can state the following. First, the meson widths, as calculated in our approximation are not strongly affected by the shape of the regulator that is used. Second, introducing WFR and LSB reduces the widths to some extent. Third, the most interesting result comes from investigating the different ways nonlocal interactions can be introduced. For sets A–C, in which the nonlocality is inspired by a separable DSE model, the widths rapidly decline at high temperatures. On the other hand, if the nonlocality is introduced via ILM, the width is a rising function of temperature. It should be noted that the latter result is also similar to what is seen in local [86] or 3D nonlocal [23] NJL studies.

Future studies should acknowledge that after the Mott transition are the two-body scattering states, rather than the resonances that play a crucial role [60]. Bearing in mind the technical difficulties encountered within the present approach, we may speculate that one possible way to proceed while still keeping the covariant setup would be to put forward the picture of complex-conjugate singularities in a Gribov–Zwanziger framework, in which they would be seen as elementary fields. From a practical point of view, such kind of modeling would use a smaller number of fictitious states. For example, recently, it has been shown that it is possible to construct bound states that have a Lehmann representation in the vacuum for a Gribov–Zwanziger model with scalar fields [92]. To our best knowledge, fermionic models of such kind are under development [36].

Alternatively, one may abandon covariant models and use a more physical "gauge," such as the Coulomb gauge, discussed, e.g., in Refs. [93,94], for describing the in-medium physics of correlations in both the hadron and the QGP phases. We shall come back to this question in a forthcoming investigation.

ACKNOWLEDGMENTS

The authors thank D. Klabučar for important contributions in the early stages of this work and for a critical reading of the manuscript. Discussions and comments by H. Grigorian, T. Hell, A. Radzhabov, N. N. Scoccola, A. Wergieluk, and D. Zablocki are gratefully acknowledged. S. B. is thankful for hospitality extended to him at the JINR Dubna and at the University of Wrocław, where much of this work was performed. D. H. is thankful for hospitality extended to him at the University of Wrocław. S. B. and D. H. received support from the Ministry of Science, Education and Sports of Croatia through Contract No. 119-0982930-1016, D. B. was supported in part by the Polish National Science Centre under Contract No. DEC-2011/02/A/ST2/00306 and by the Russian Fund for Basic Research under Grant No. 11-02-01537-a, while G. C. is grateful for support by CONICET (Argentina). This work was supported in part by CompStar, a Research Networking Programme of the European Science Foundation, and by CompStar-POL, a grant from the Polish Ministry for Science and Higher Education supporting it.

APPENDIX: POLARIZATION FUNCTION AT FINITE TEMPERATURE

In this Appendix, the derivation of the imaginary part of the in-medium polarization function (56) will be performed. For clarity, we study the case in which $\mu = 0$, $\varphi_3 = 0$ and the mesons are at rest $\mathbf{q} = 0$. By analytically continuing $\omega_n \to -iz$, and using $\nu_m = -iq_0$, the integrand of the polarization function takes the form

$$\pi_M(z) = f^2(-z^2 + \mathbf{p}^2)\frac{K_M(-z^2, \mathbf{p}^2, -q_0^2, 0)}{\mathcal{D}(-z_+^2, \mathbf{p}^2)\mathcal{D}(-z_-^2, \mathbf{p}^2)}, \quad \text{(A1)}$$

where $z_\pm = z \pm \frac{q_0}{2}$ and where we suppressed the $\mathbf{p}$ and q_0 dependence of π_M for brevity. The master formula for Matsubara summation is then

$$\begin{aligned} -2\pi i T \sum_{n=-\infty}^{\infty} \pi_M\left(i\omega_n - \frac{i\nu_m}{2}\right) &= \int_{i\infty}^{-i\infty} dz \pi_M(z) + \int_{-i\infty+\delta}^{i\infty+\delta} dz \pi_M(z) n(z_+) \\ &\quad - \int_{-i\infty-\delta}^{i\infty-\delta} dz \pi_M(z) n(-z_+), \end{aligned} \quad \text{(A2)}$$

where on the left-hand side we used translational invariance, with $n(z) = (1 + e^{\beta z})^{-1}$ and $\delta > 0$ infinitesimal. It is crucial to observe that the integrals can be performed using the information on the singularity structure of the propagator in the whole complex plane. Although these can be rather complicated, we shall assume that, at some not-too-high temperature, the only singularities are simple poles at m_{qp}; see the previous discussion in the text. Then, the only singularities of the propagator that we need to worry about are $\pm E_{\mathrm{qp}}^{\pm}$, where $E_{\mathrm{qp}} = \sqrt{v_{\mathrm{qp}}^2 \mathbf{p}^2 + m_{\mathrm{qp}}^2}$, and $E_{\mathrm{qp}}^a = E_{\mathrm{qp}} + a q_0/2$, with $a = \pm$.

Evaluating the first integral by closing the contour with a large semicircle at $\mathrm{Re}(z) > 0$, we obtain

$$\int_{i\infty}^{-i\infty} dz \pi_M(z) = 2\pi i \sum_{a=\pm} \mathrm{Res}(E_{\mathrm{qp}}^a),$$

where

$$\mathrm{Res}(E^a_{\mathrm{qp}}) = -\frac{f^2(-(E^a_{\mathrm{qp}})^2+\mathbf{p}^2)}{2E_{\mathrm{qp}}}\frac{K_M(-(E^a_{\mathrm{qp}})^2,\mathbf{p}^2,-q_0^2,0)}{\mathcal{D}'(-E^2_{\mathrm{qp}},\mathbf{p}^2)\mathcal{D}(-(E_{\mathrm{qp}}+aq_0)^2,\mathbf{p}^2)}. \tag{A3}$$

Here, we denoted

$$\mathcal{D}'(p^2) = \partial\mathcal{D}/\partial p^2. \tag{A4}$$

Since the distribution function $n(z)$ has poles only on the imaginary axis, the evaluation of the remaining integrals is performed in a similar way. The only subtle step is acknowledging that $n(z\pm q_0) = n(z\pm i\nu_m) = n(z)$. For Eq. (A2), we obtain

$$T\sum_{n=-\infty}^{\infty}\pi_M\left(i\omega_n - \frac{i\nu_m}{2}\right) = -[1-2n(E_{\mathrm{qp}})]\sum_{a=\pm}\mathrm{Res}(E^a_{\mathrm{qp}}), \tag{A5}$$

where we have used that $\mathrm{Res}(E^a_{\mathrm{qp}}) = -\mathrm{Res}(-E^a_{\mathrm{qp}})$.

The imaginary part develops from the point where $E_{\mathrm{qp}} = q_0/2$, which, owing to fact that we deal with real poles, can be handled by the $i\epsilon$ prescription. To obtain Eq. (63), it is sufficient to calculate

$$\begin{aligned}\mathrm{Res}(E^-_{\mathrm{qp}}+i\epsilon) - \mathrm{Res}(E^-_{\mathrm{qp}}-i\epsilon) = &-\frac{f^2(-(E^-_{\mathrm{qp}})^2+\mathbf{p}^2)}{2E_{\mathrm{qp}}}\frac{K_M(-(E^-_{\mathrm{qp}})^2,\mathbf{p}^2,-q_0^2,0)}{\mathcal{D}'(-E^2_{\mathrm{qp}},\mathbf{p}^2)}\\ &\times\left[\frac{1}{\mathcal{D}(-(E_{\mathrm{qp}}-q_0+i\epsilon)^2,\mathbf{p}^2)} - \frac{1}{\mathcal{D}(-(E_{\mathrm{qp}}-q_0-i\epsilon)^2,\mathbf{p}^2)}\right],\end{aligned} \tag{A6}$$

where we have used the fact that the only discontinuities arise from the denominator. By expanding around $E_{\mathrm{qp}} = q_0/2$,

$$\mathcal{D}(-(E_{\mathrm{qp}}-q_0-i\epsilon)^2,\mathbf{p}^2) \to 2q_0(E^-_{\mathrm{qp}}\mp i\epsilon)\mathcal{D}'(-q_0^2/4,\mathbf{p}^2),$$

and using the Plemelj formula, the following discontinuity develops:

$$\mathrm{Res}(E^-_{\mathrm{qp}}+i\epsilon) - \mathrm{Res}(E^-_{\mathrm{qp}}-i\epsilon) = \frac{f^2(-(E^-_{\mathrm{qp}})^2+\mathbf{p}^2)}{4q_0E_{\mathrm{qp}}}\frac{K_M(-(E^-_{\mathrm{qp}})^2,\mathbf{p}^2,-q_0^2,0)}{\mathcal{D}'(-E^2_{\mathrm{qp}},\mathbf{p}^2)\mathcal{D}'(-q_0^2/4,\mathbf{p}^2)}(-2i\pi)\delta(E^-_{\mathrm{qp}}). \tag{A7}$$

Plugging Eq. (A7) into Eq. (A5) and back into the original formula (56) for the polarization function yields

$$\mathrm{Im}[\Pi_M(-iq_0)] = \frac{d_q}{16\pi}[1-2n(q_0/2)]\sqrt{1-\left(\frac{2m_{\mathrm{qp}}}{q_0}\right)^2}f^2\left(\frac{q_0^2}{4}-m^2_{\mathrm{qp}}\right)\frac{K_M\left(0,\frac{q_0^2}{4}-m^2_{\mathrm{qp}},-q_0^2,0\right)}{\left[\mathcal{D}'\left(-\frac{q_0^2}{4},\frac{q_0^2}{4}-m^2_{\mathrm{qp}}\right)\right]^2}\theta\left(\frac{q_0}{2}-m_{\mathrm{qp}}\right). \tag{A8}$$

Introducing the chemical potential and the Polyakov loop is now a simple matter. By generalizing $2n(z) \to n^\Phi_+(z) + n^\Phi_-(z)$, one arrives at Eq. (64).

[1] E. V. Shuryak, Nucl. Phys. **A750**, 64 (2005).
[2] U. A. Wiedemann, Nucl. Phys. **A904–A905**, 3c (2013).
[3] A. Sorin, V. Kekelidze, A. Kovalenko, R. Lednicky, I. Meshkov, and G. Trubnikov, Nucl. Phys. **A855**, 510 (2011).
[4] M. Bleicher, M. Nahrgang, J. Steinheimer, and P. Bicudo, Acta Phys. Polon. B **43**, 731 (2012).
[5] K. Fukushima and T. Hatsuda, Rep. Prog. Phys. **74**, 014001 (2011).
[6] K. Fukushima, J. Phys. G **39**, 013101 (2012).
[7] S. Borsanyi, Nucl. Phys. **A904–A905**, 270c (2013).
[8] F. Karsch, K. Redlich, and A. Tawfik, Phys. Lett. B **571**, 67 (2003).
[9] F. Karsch, K. Redlich, and A. Tawfik, Eur. Phys. J. C **29**, 549 (2003).
[10] R. Hagedorn, Nuovo Cimento Suppl. **3**, 147 (1965).

[11] S. Borsányi, Z. Fodor, C. Hoelbling, S. D. Katz, S. Krieg, C. Ratti, and K. K. Szabó (Wuppertal-Budapest Collaboration), J. High Energy Phys. 09 (**2010**) 073.
[12] Y. Nambu and G. Jona-Lasinio, Phys. Rev. **122**, 345 (1961).
[13] Y. Nambu and G. Jona-Lasinio, Phys. Rev. **124**, 246 (1961).
[14] S. Klimt, M. F. M. Lutz, U. Vogl, and W. Weise, Nucl. Phys. **A516**, 429 (1990).
[15] S. P. Klevansky, Rev. Mod. Phys. **64**, 649 (1992).
[16] T. Hatsuda and T. Kunihiro, Phys. Rep. **247**, 221 (1994).
[17] M. Buballa, Phys. Rep. **407**, 205 (2005).
[18] C. D. Roberts and S. M. Schmidt, Prog. Part. Nucl. Phys. **45**, S1 (2000).
[19] R. Alkofer and L. von Smekal, Phys. Rep. **353**, 281 (2001).
[20] C. S. Fischer, J. Phys. G **32**, R253 (2006).
[21] P. C. Tandy, Prog. Part. Nucl. Phys. **39**, 117 (1997).
[22] C. S. Fischer, Phys. Rev. Lett. **103**, 052003 (2009).
[23] S. M. Schmidt, D. Blaschke, and Y. L. Kalinovsky, Phys. Rev. C **50**, 435 (1994).
[24] R. D. Bowler and M. C. Birse, Nucl. Phys. **A582**, 655 (1995).
[25] R. S. Plant and M. C. Birse, Nucl. Phys. **A628**, 607 (1998).
[26] D. Blaschke and P. C. Tandy, in Proceedings of the International Workshop on Understanding deconfinement in QCD, edited by D. Blaschke, F. Karsch, and C. D. Roberts (World Scientific, Singapore, 2000), p. 218.
[27] D. Blaschke, G. Burau, Y. L. Kalinovsky, P. Maris, and P. C. Tandy, Int. J. Mod. Phys. A **16**, 2267 (2001).
[28] I. General, D. Gomez Dumm, and N. N. Scoccola, Phys. Lett. B **506**, 267 (2001).
[29] D. Gomez Dumm and N. N. Scoccola, Phys. Rev. D **65**, 074021 (2002).
[30] D. Gomez Dumm and N. N. Scoccola, Phys. Rev. C **72**, 014909 (2005).
[31] D. Blaschke, D. Horvatic, D. Klabucar, and A. E. Radzhabov, Bled Workshops in Physics (2006), Vol. **7**, 1, p. 20.
[32] M. B. Parappilly, P. O. Bowman, U. M. Heller, D. B. Leinweber, A. G. Williams, and J. B. Zhang, Phys. Rev. D **73**, 054504 (2006).
[33] D. Blaschke, Y. L. Kalinovsky, and P. C. Tandy, arXiv:hep-ph/9811476.
[34] M. Bhagwat, M. A. Pichowsky, and P. C. Tandy, Phys. Rev. D **67**, 054019 (2003).
[35] D. Dudal, J. A. Gracey, S. P. Sorella, N. Vandersickel, and H. Verschelde, Phys. Rev. D **78** 065047 (2008).
[36] D. Dudal, M. S. Guimaraes, L. F. Palhares, and S. P. Sorella, arXiv:1303.7134.
[37] D. Blaschke, Y. L. Kalinovsky, G. Roepke, S. M. Schmidt, and M. K. Volkov, Phys. Rev. C **53** 2394 (1996).
[38] E. Ruiz Arriola and L. L. Salcedo, Phys. Lett. B **450** 225 (1999).
[39] M. Buballa and S. Krewald, Phys. Lett. B **294** 19 (1992).
[40] D. Gomez Dumm, A. G. Grunfeld, and N. N. Scoccola, Phys. Rev. D **74** 054026 (2006).
[41] G. Ripka, *Quarks Bound by Chiral Fields: The Quark-Structure of the Vacuum and of Light Mesons and Baryons* (Clarendon, Oxford, 1997), p. 205.
[42] T. Schäfer and E. V. Shuryak, Rev. Mod. Phys. **70** 323 (1998).
[43] D. Blaschke, M. Buballa, A. E. Radzhabov, and M. K. Volkov, Yad. Fiz. **71**, 2012 (2008); , [Phys. At. Nucl. **71**, 1981 (2008)].
[44] G. A. Contrera, D. Gomez Dumm, and N. N. Scoccola, Phys. Lett. B **661**, 113 (2008).
[45] T. Hell, S. Roessner, M. Cristoforetti, and W. Weise, Phys. Rev. D **79**, 014022 (2009).
[46] S. Noguera and N. N. Scoccola, Phys. Rev. D **78**, 114002 (2008).
[47] T. Hell, S. Rossner, M. Cristoforetti, and W. Weise, Phys. Rev. D **81**, 074034 (2010).
[48] G. A. Contrera, M. Orsaria, and N. N. Scoccola, Phys. Rev. D **82**, 054026 (2010).
[49] D. Horvatic, D. Blaschke, D. Klabucar, and O. Kaczmarek, Phys. Rev. D **84**, 016005 (2011).
[50] A. E. Radzhabov, D. Blaschke, M. Buballa, and M. K. Volkov, Phys. Rev. D **83**, 116004 (2011).
[51] T. Hell, K. Kashiwa, and W. Weise, Phys. Rev. D **83**, 114008 (2011).
[52] K.-I. Kondo, Phys. Rev. D **82**, 065024 (2010).
[53] D. Gomez Dumm, D. B. Blaschke, A. G. Grunfeld, and N. N. Scoccola, Phys. Rev. D **73**, 114019 (2006).
[54] A. H. Rezaeian and H.-J. Pirner, Nucl. Phys. **A769**, 35 (2006).
[55] J. Hüfner, S. P. Klevansky, P. Zhuang, and H. Voss, Ann. Phys. (N.Y.) **234**, 225 (1994).
[56] P. Zhuang, J. Hüfner, and S. P. Klevansky, Nucl. Phys. **A576**, 525 (1994).
[57] J. Hüfner, S. P. Klevansky, and P. Rehberg, Nucl. Phys. **A606**, 260 (1996).
[58] D. Blaschke, J. Berdermann, J. Cleymans, and K. Redlich, Few-Body Syst. **53**, 99 (2012).
[59] L. Turko, D. Blaschke, D. Prorok, and J. Berdermann, Acta Phys. Pol. B Proc. Suppl. **5**, 485 (2012).
[60] A. Wergieluk, D. Blaschke, Y. L. Kalinovsky, and A. Friesen, arXiv:1212.5245.
[61] K. Yamazaki and T. Matsui, Nucl. Phys. A **913**, 19 (2013).
[62] D. Blaschke, D. Zablocki, M. Buballa, and G. Roepke, arXiv:1305.3907.
[63] C. J. Burden, L. Qian, C. D. Roberts, P. C. Tandy, and M. J. Thomson, Phys. Rev. C **55**, 2649 (1997).
[64] J. I. Kapusta, *Finite Temperature Field Theory* (Cambridge University, Cambridge, England, 1989).
[65] J. M. Cornwall, R. Jackiw, and E. Tomboulis, Phys. Rev. D **10**, 2428 (1974).
[66] A. Bender, D. Blaschke, Y. Kalinovsky, and C. D. Roberts, Phys. Rev. Lett. **77**, 3724 (1996).
[67] D. Blaschke and C. D. Roberts, Nucl. Phys. **A642**, c197 (1998).
[68] J. A. Mueller, C. S. Fischer, and D. Nickel, Eur. Phys. J. C **70**, 1037 (2010).
[69] S.-X. Qin, L. Chang, Y.-X. Liu, and C. D. Roberts, Phys. Rev. D **84**, 014017 (2011).
[70] O. K. Kalashnikov, Pis'ma Zh. Eksp. Teor. Fiz. **41**, 477 (1985) [, JETP Lett. **41**, 582 (1985)].
[71] A. M. Polyakov, Phys. Lett. **B72**, 477 (1978).
[72] S. Roessner, C. Ratti, and W. Weise, Phys. Rev. D **75**, 034007 (2007).
[73] S. Benic, D. Blaschke, and M. Buballa, Phys. Rev. D **86**, 074002 (2012).

[74] K. Yagi, T. Hatsuda, and Y. Miake, Cambridge Monogr. Part. Phys., Nucl. Phys., Cosmol. **23**, 1 (2005).
[75] A. Actor, Nucl. Phys. **B265**, 689 (1986).
[76] O. Kaczmarek, F. Karsch, E. Laermann, C. Miao, S. Mukherjee, P. Petreczky, C. Schmidt, W. Soeldner, and W. Unger, Phys. Rev. D **83**, 014504 (2011).
[77] G. A. Contrera, A. G. Grunfeld, and D. B. Blaschke, arXiv:1207.4890.
[78] D. Horvatic, D. Blaschke, D. Klabucar, and A. E. Radzhabov, Phys. Part. Nucl. **39**, 1033 (2008).
[79] S. Ejiri, Nucl. Phys. B, Proc. Suppl. **94**, 19 (2001).
[80] B.-J. Schäfer, J. M. Pawlowski, and J. Wambach, Phys. Rev. D **76**, 074023 (2007).
[81] T. Hell, K. Kashiwa, and W. Weise, J. Mod. Phys. **4**, 644 (2013).
[82] J. P. Carlomagno, D. G. Dumm, and N. N. Scoccola, Phys. Rev. D **88**, 074034 (2013).
[83] A. Scarpettini, D. Gomez Dumm, and N. N. Scoccola, Phys. Rev. D **69**, 114018 (2004).
[84] G. A. Contrera, D. G. Dumm, and N. N. Scoccola, Phys. Rev. D **81**, 054005 (2010).
[85] R. E. Cutkosky, P. V. Landshoff, D. I. Olive, and J. C. Polkinghorne, Nucl. Phys. **B12**, 281 (1969).
[86] H. Hansen, W. M. Alberico, A. Beraudo, A. Molinari, M. Nardi, and C. Ratti, Phys. Rev. D **75**, 065004 (2007).
[87] W. Florkowski and B. L. Friman, Z. Phys. A **347**, 271 (1994).
[88] W. Florkowski and B. L. Friman, Acta Phys. Polon. B **25** 49 (1994).
[89] S. Strauss, C. S. Fischer, and C. Kellermann, Phys. Rev. Lett. **109** 252001 (2012).
[90] A. Windisch, R. Alkofer, G. Haase, and M. Liebmann, Comput. Phys. Commun. **184**, 109 (2013).
[91] A. Windisch, M. Q. Huber, and R. Alkofer, Phys. Rev. D **87** 065005 (2013).
[92] M. A. L. Capri, D. Dudal, M. S. Guimaraes, L. F. Palhares, and S. P. Sorella, Int. J. Mod. Phys. A **28**, 1350034 (2013).
[93] M. Pak and H. Reinhardt, Phys. Lett. B **707**, 566 (2012).
[94] P. Watson and H. Reinhardt, Phys. Rev. D **86**, 125030 (2012).